DOE/NV/03624--0968

Nevada National Security Site

Wolfsbane Multi-Probe Ejecta Diagnostic

Conceptual experimental diagnostic design report
December 29, 2020

Office of Experimental Science Campaign 3
Advanced Diagnostics

Level 2 Milestone MRT 7110

Stuart Baker and Andrew Corredor
Daniel Clayton, Logan Fegenbush, Amy Lewis, Robert Malone,
David Phillips, Vincent Romero, Duane Smalley, Sheriden Smith,
Dan Sorenson, Katherine Walters

This work was done by Mission Support and Test Services, LLC, under
Contract No. DE-NA0003624 with the U.S. Department of Energy.

NNSA Advanced Diagnostics Program Level 2 Milestone MRT 7110 – Wolfsbane Multi-Probe Ejecta Diagnostic

This report serves as the deliverable for Level 2 Milestone MRT 7110.

MRT 7110 Project Description – This milestone will develop a conceptual design for a multi-pulse, soft x-ray source with reduced parallax to better assess the progression of material motion along with a demonstration of ejecta imaging with two wavelength, visible shadowgraphy designed to record the same line-of-sight field of view as the x-ray system. This capability would support experiments at U1a, STL, LANL, or LLNL on material eject under different shock pressures, providing feedback into hydrodynamic material modeling of mix.

MRT 7110 Exit Criteria – Submit a technical report on conceptual design for a future Wolfsbane diagnostic.

MRT 7110 Stretch Goal (requested by Advanced Diagnostics federal program manager due to extending and staggering the various institutional delivery dates. NNSS delivery date was extended one quarter to have new due date of the first quarter of each fiscal year) – Demonstration of a multi-pulse Platts source to reduce the four-pulse system parallax.

This work is produced in the NNSS Transformational Diagnostics and Imaging (TDI) group for the Radiography and Advanced Imaging Development (RAID) project in support of the NNSA Office of Experimental Science Campaign 3 Advanced Diagnostics program.

CONTENTS

1. EXECUTIVE SUMMARY

The Nevada National Security Site (NNSS) has designed a diagnostic to provide increased information on the behavior of plutonium ejecta in explosively driven double shock systems. We intend to implement this new diagnostic capability on the Red Sage Wolfsbane experiment series to be scheduled after FY 2025.

The aim of the Red Sage campaign of subcritical experiments (SCEs) is to measure the dynamic characteristics of plutonium ejecta. Nightshade, occurring in FY 2021 at the NNSS, will be followed by Wolfsbane and Hemlock. Diagnostics on the Nightshade experiments are quantifying the source term for the ejecta emission density into vacuum using two Cygnus 1.8 MeV x-ray radiographs. These diagnostics will not diagnose ejecta particle size.

The NNSS Radiography and Advanced Imaging Development (RAID) group is pursuing a new multi-pulse 200 keV soft x-ray source with reduced parallax that will be combined with the digital Kraken camera that produces eight frames of continuous images. The ejecta density measurements, plus this new two-wavelength shadowgraphy method, will be used to constrain ejecta particle distribution size.

Because SCEs are executed inside a confinement vessel, we face the added challenge of getting soft x-rays into the vessel and images out. At this juncture, our work needs to consider and resolve the items below.

- Multi-pulse soft x-ray source along with the vessel interface needs to be developed and evaluated.
- The new Kraken camera is in its infancy and needs to be elevated to full resolution.
- The radiographic imaging chain, including scintillator and optical image relay, needs to be designed and trial tested.
- The two-wavelength shadowgraphy method requires a special light source synchronized with radiographs and an eight-frame digital framing Kraken camera readout to capture a long record of the ejecta motion.
- Two-wavelength shadowgraphy needs to go through a blind testing phase to qualify analysis codes.

Our new Wolfsbane diagnostic will help constrain longstanding issues on the characteristics of ejecta and the effect on mix models of converging systems, while providing comprehensive information on ejecta density and illusive particle size detail. This new x-ray source combined with the digital framing Kraken camera will provide a new capability for soft radiography tests across the complex.

2. INTRODUCTION

The Red Sage campaign is a series of subcritical dynamic plutonium experiments designed to measure ejecta. Nightshade is the first of three Red Sage experimental series to be followed by Wolfsbane and Hemlock series in later years. The Nightshade series is a baseline set of experiments that will measure the amount of ejecta emission into vacuum from a double-shocked plutonium surface. The Nightshade series will provide meaningful constraints on the source term in physics-based ejecta models [1].

The three tests Nightshade A, B, and C are being executed at the Nevada National Security Site (NNSS) U1a facility in fiscal year (FY) 2021.

The Nightshade double-shock drive consists of a plane-wave high-explosive (HE) lens, a tantalum anvil, and a target to provide shock to the plutonium surface. The explosive load and plutonium mass of each drive is rather low. To more efficiently use the vessel and facility, we are incorporating multiple explosive drives with targets into one experiment. While this approach makes the Nightshade diagnostics more complex, it vastly increases the data return without adding more shots [2].

The two key measurements needed to better constrain ejecta mix models for various shock pressures are the density and particle size of the ejecta. We are pursuing solutions to make these types of measurements on the Red Sage Wolfsbane series.

3. BACKGROUND

3.1. Silverleaf and PIPEX soft radiography demonstration

Silverleaf, a confirmatory test series, helped validate a preliminary experiment configuration to measure required Red Sage parameters. The Silverleaf series was executed at the Los Alamos National Laboratory (LANL) in July and August 2016 to demonstrate a prototype of the Nightshade package with HE drives on surrogate materials and a suite of preliminary diagnostics. The experimental package is illustrated in Fig. 3.1

Radiography is often used to measure the material density in these types of dynamic explosive tests. Lower energy, softer spectrum x-rays are needed to resolve contrast in the relatively low-density ejecta radiography. Multi-pulse x-ray sources with timed sequence radiographs are also desired to provide better information on the evolution of the test.

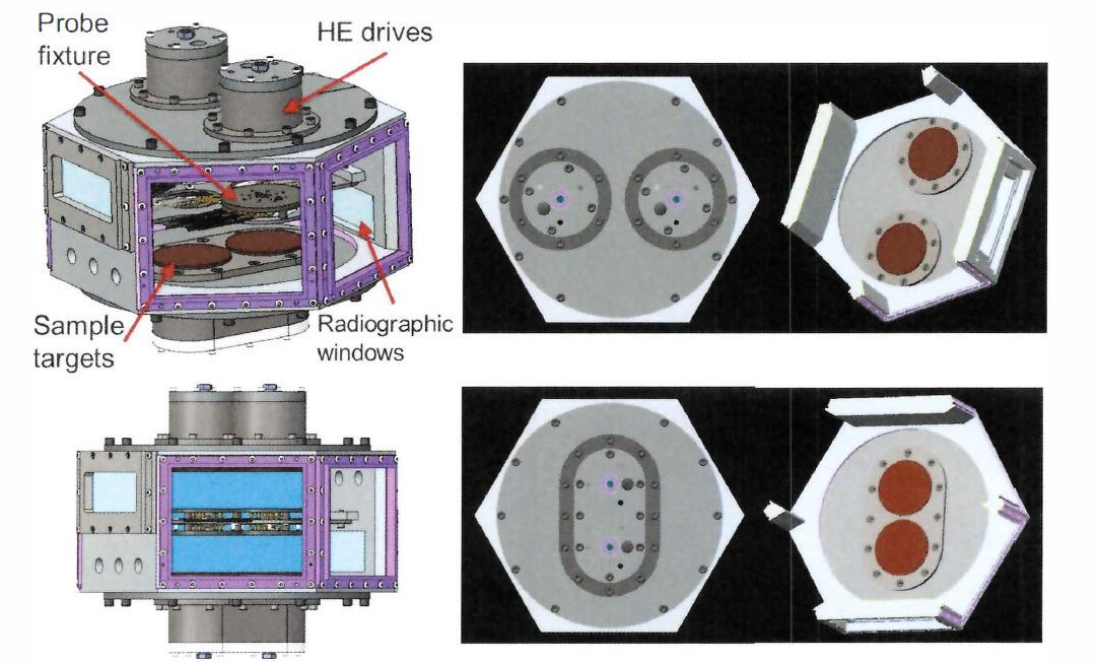

Figure 3.1. Radiographic view of the package. The diagnostic mounting plate is 35 mm above the targets.

For the Silverleaf series the NNSS radiography team configured a two-pulse soft source with two Supersaver Marx generators and two separate diodes in the x-ray source head. The images were recorded on a three-frame digital hybrid CMOS camera. The Supersaver Marx, with estimated endpoint energy of ~250 keV, and imaging system provided good contrast on the ejecta test (Figs. 3.2 and 3.3).

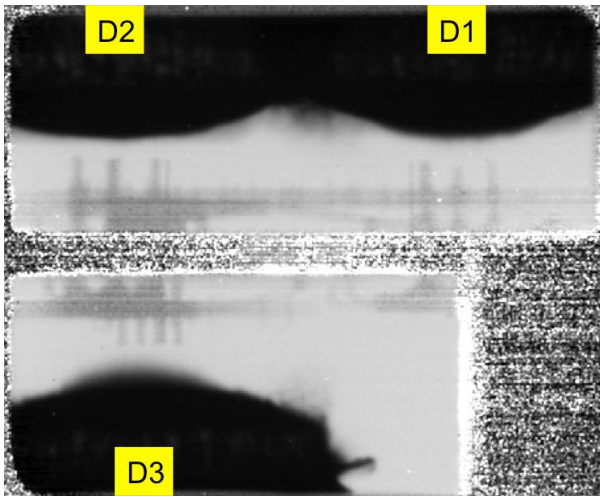

Figure 3.2. Late-time radiography (ratio of raw data to the static) of the three physics packages for the Silverleaf D experiment. Ejecta can clearly be seen for the D3 package at the bottom left of the image. Edge jetting is observed in the image, but appears to be outside the ejecta region.

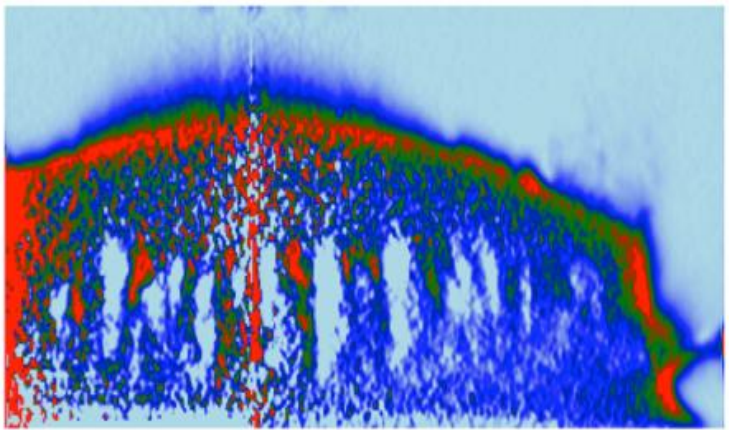

Figure 3.3. Abel inversion of the package D3 shown in Fig. 3.2. Ejecta mass densities are easily extracted from the data.

After Silverleaf, the plan was to develop a four-pulse Supersaver Marx source to use on Nightshade radiography. The NNSS team developed a four-pulse zigzag head with four separate diode point sources in the x-ray head and demonstrated this design on PIPEX tests [3] at the United Kingdom Atomic Weapons Establishment (AWE) in 2017. The four-pulse source radiographs were recorded on an older electro-static image tube–based four-frame camera.

This four-shooter radiography system was showing good performance for low-density material scene contrast. The sensitivity for Silverleaf was estimated to be <1 mg/cm^2. In a previous study [4], which used the Supersaver sources and a molybdenum anode, sensitivities were estimated to be as low as 0.05 mg/cm^2.

3.2. Radiography design for Nightshade at U1a

For final Nightshade radiography design, the separate anode and physical spacing in the four-shooter system were a concern, as they resulted in a parallax effect in the radiographs [5]. Another major concern was the vessel confinement modification that would be required to field the four-shooter x-ray head on the 3-foot vessel experiment at U1a. The approved vessel confinement windows are 0.5-inch-thick aluminum. These thick windows attenuate lower-energy x-rays, which is acceptable for Cygnus 2.3 MeV endpoint radiography, but is not acceptable for the softer spectrum of the 250 keV Supersavers. Under this condition, because almost all of the low-energy Supersaver source would be attenuated in the vessel window there would not be enough energy left to radiograph the experiment. Therefore, the NNSS team researched, tested and proposed an alternate, thinner vessel window confinement material; however, the LANL vessel approving authority did not have adequate time in the schedule to authorize the use of different windows on Nightshade.

3.3. Cygnus radiography is utilized on the Nightshade series

To accomplish the primary diagnostic, radiography, using the approved vessel configuration, we had to tune the Cygnus rod-pinch diode to a slightly softer spectrum and dose for Nightshade. Testing was done on Mercury and Cygnus to qualify the lower-energy rod-pinch diode illustrated in Fig. 3.4.

The standard Cygnus tungsten rod-pinch diode delivers 4 rad at 1 m burst of x-rays with a peak energy ~1 MeV and a 2.3 MeV end-point energy, ideal for measuring line densities up to around 100 g/cc. For the Nightshade series, the tungsten rod was replaced with a titanium rod to produce a slightly softer 1.8 MeV end-point spectrum with dose of 1 rad at 1 m for the ejecta radiographs.

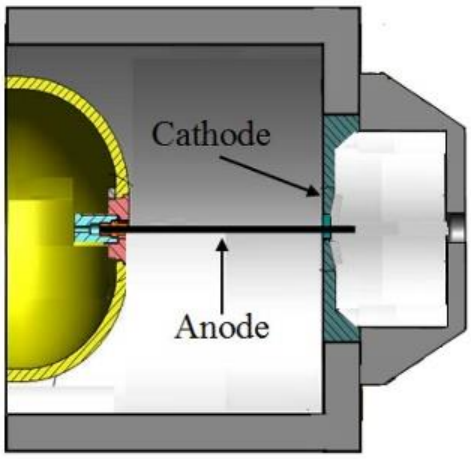

Figure 3.4. Cross section of the Cygnus rod-pinch diode.

3.4. Recent multi-pulse soft x-ray radiography tests

The four-pulse soft radiography platform NNSS Transformational Diagnostics and Imaging (TDI) developed for the Red Sage subcritical series has been successfully deployed on a number of dynamic tests [6]. After the AWE PIPEX experiment in the UK (2017), the multiple sources supported a number of experimental activities, two examples being a two-pulse configuration imaging a series of smaller tests at the NNSS Special Technologies Laboratory Boom Box and at LANL's proton radiography (pRad) facility in support of Advanced Diagnostics multi-probe radiography (MRT 7109) efforts in 2020.

In early October 2020 the LANL pRad team, NNSS TDI, and the Army Research Lab conducted the first transverse radiography test on an electrically burst wire experiment. Twenty-one frames of proton radiography along the *z*-axis captured the

magnetic field generated. Three frames of soft radiography along the *y*-axis captured the metal as it burst. One hundred twenty-eight frames of visible imaging along the *x*-axis captured the gas cloud expansion. Soft radiography was fielded with NNSS Supersaver Marx banks cable coupled to our multi-pulse zigzag x-ray diode head. Tungsten anodes having a 1.59 mm diameter were used for this experiment. Radiographic images were acquired with the new NNSS Kraken digital 8-frame hybrid CMOS camera that was lens coupled to image and record the radiographs from a thallium-doped cesium iodide (CsI:Tl) scintillator screen. The photos of the experimental hardware are shown in Figs. 3.5, 3.6, and 3.7.

Figure 3.5. NNSS TDI multi-pulse flash x-ray system fielding setup at the LANL pRad facility. Four Marx generators, positioned in the lower left, are shielded from the beam line. Long, high-voltage cable transmission lines are shown connected to the x-ray diode head assembly in the experimental area in the pRad beam line.

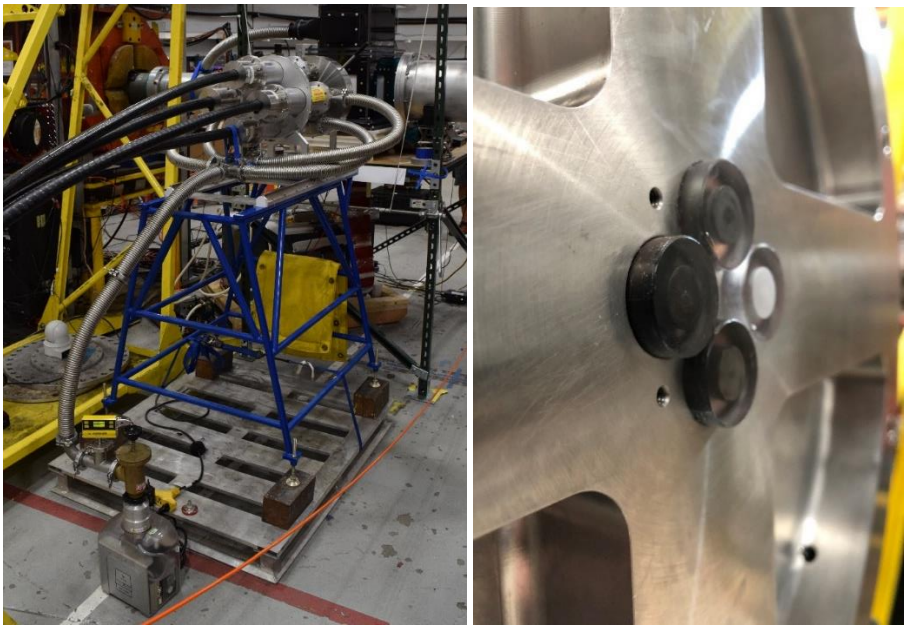

Figure 3.6. Left: Multi-pulse diode on positioning stand preparing for the tests at the pRad facility. Right: Front of the multi-pulse diode head showing position of 4 anodes (behind polycarbonate windows).

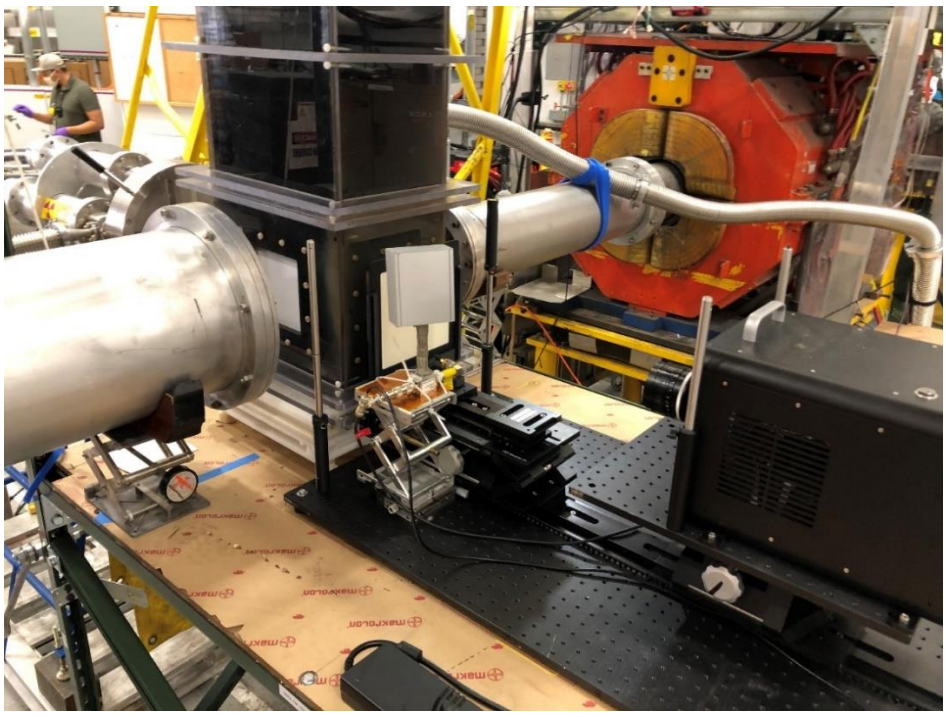

Figure 3.7. Imaging setup with Kraken camera, shown in the lower right (black box). The Kraken camera is lens coupled to image a CsI:Tl white square scintillator screen in the lower section of the experiment tower structure positioned in the pRad beam line. The soft x-ray source is in the upper left on the far side of the experiment structure.

3.5. Current designs for multi-pulse low-energy x-ray systems

Previous generations of flash x-ray sources typically use pulsed power systems with a diode to generate high-energy bremsstrahlung x-rays. Softer x-ray sources, with endpoint energies in the hundreds of kiloelectron volts, are often used to radiograph focused experiments with lower line densities of (0.1–10 g/cc) than those found in typical scaled experiments. Soft x-ray sources operate in a fashion similar to the higher-energy sources, typically using a Marx bank to create a short (tens of nanoseconds), high-voltage (hundreds of kilovolts) pulse across a diode similar in design to the rod-pinch. These sources, based on previous designs [7] developed for the Pegasus and Atlas facilities, (often referred to as Platts Flash Marx Banks) have been used for decades on a wide range of experiments [8, 9]. The current design used by NNSS is a portable, 37-stage Marx bank, called Supersaver, with the capacitor stages charged to –30 kV and discharged over a needle-and-washer diode through a 40-ohm, coaxial transmission line [9]. This flexible transmission line, shown in Fig. 3.8, allows the Marx bank to be located away from the experiment in a shielded area.

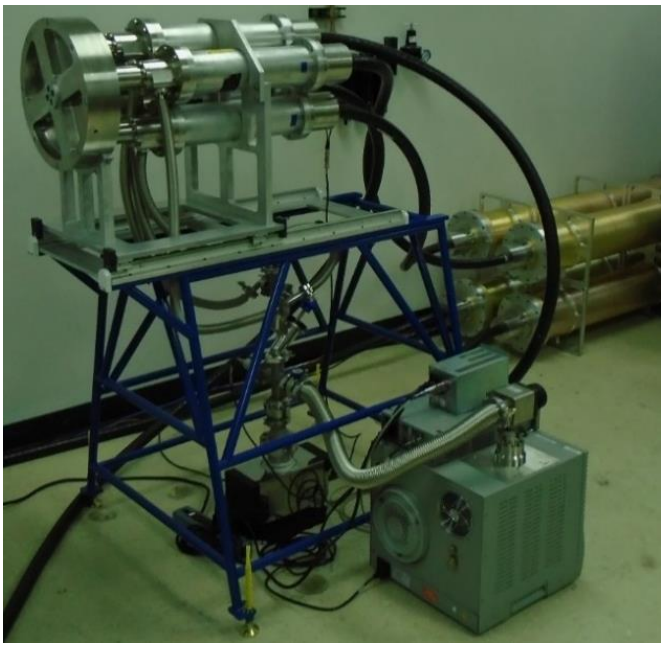

Figure 3.8. Photo of a modern four-pulse soft x-ray head with Supersaver Marx banks in background.

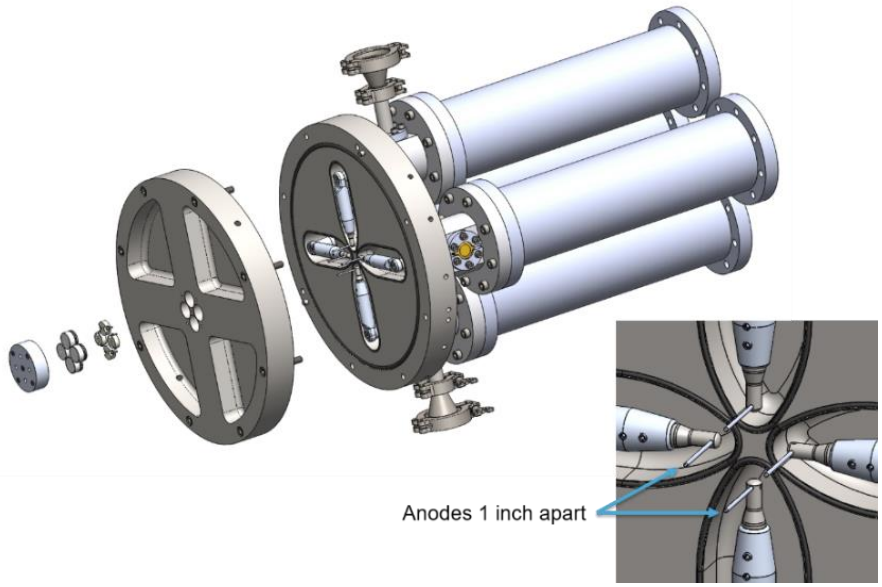

Figure 3.9 The x-ray head CAD model illustration shows the design placing four anodes as close together as possible to minimize parallax in radiographs from the four separate point sources.

This system delivers one to four independently triggered flash x-ray pulses at 400 keV with a 35 ns pulse width. The anodes are positioned to minimize image parallax, with each anode located on the corner of a 23 × 23 mm square as shown in Fig. 3.9.

The latest version of the four-pulse soft source head design is shown in Fig. 3.9. This source design has been considered for arranging the x-ray head in an experiment confinement vessel as shown in Fig. 3.10 to avoid x-ray attenuation of the vessel window. The source parallax problem would be amplified in this configuration and the diode head would also need extensive design modification for the vessel interface. This design concept was never pursued.

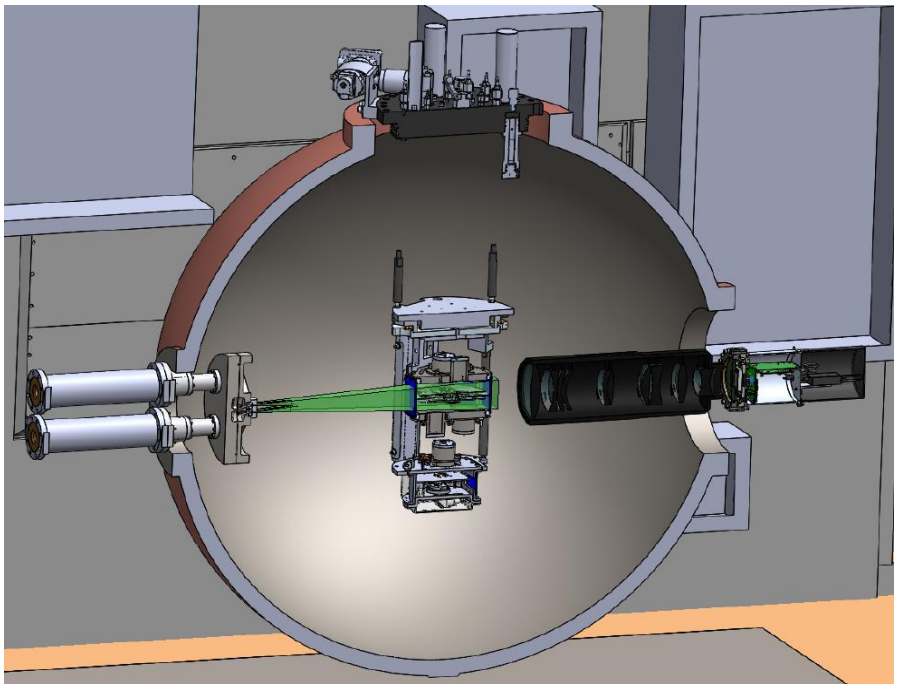

Figure 3.10. Conceptual design for in-vessel multi-pulse soft x-ray source with an optical image relay lens to a multi-frame camera to record ejecta radiographs.

4. WOLFSBANE DIAGNOSTIC DEVELOPMENT

4.1. Multi-pulse radiography source development

Research is now focused on developing multi-pulse, single-anode diode designs that will image dynamic tests without the parallax effect present in current designs. Marx banks to test the pulse-adder are currently being fabricated. These banks, connected to the x-ray diode with high-voltage cables, will test the pulsed power coupling efficiency and impedance matching. Later in 2021 multi-pulse x-ray emission will be tested at NNSS TDI. Different diode designs will be evaluated in the lab to determine the effects of plasma buildup in the diode between pulses and to determine which design produces the cleanest pulses. The multi-pulse x-ray emission will be tested for spot size and dose while the source will also be viewed with an x-ray pinhole camera to evaluate the characteristics of the diode performance. Successful development of a multi-pulse single diode will eliminate parallax issues associated with the separate diode configuration.

Future work in following years will pursue high-voltage vacuum feedthroughs to deliver the pulse to an x-ray diode head inside a confinement vessel. This will eliminate the need for x-ray blast windows, which are both a risk to vessel confinement and a strong attenuator of the x-rays. This arrangement would also allow placement of the x-ray diode closer to the object, thereby allowing increased dose and magnification.

4.2. Low-energy x-ray source technologies

The NNSS Source Development project is developing next-generation sources to produce brighter, higher-resolution, multi-pulse soft x-ray radiographs. Lower-energy multi-pulse sources are needed for multiple types of experiments such as ejecta measurements, detonator initiation tests, or dynamic x-ray diffraction tests.

In an effort to produce the next-generation low-energy source system, the NNSS is working with Applied Physical Electronics, L.C. (APELC) of Austin, Texas, to design and fabricate modular compact Marx generators and a pulse adder system that will be able to couple multiple sources with a single transmission line. These efforts are described next.

4.2.1. Marx generators

Modular, compact Marx generator designs are desired for use in experiments being conducted at numerous facilities. Marx generators currently used in our experimental testbeds are often problematic when deployed on multi-pulse systems, and issues range

from large footprints to cumbersome ancillary components. These sources use a pulse-forming-line (PFL) to deliver energy to the load at a matched impedance. Because of the physical length needed to store a useable amount of energy and deliver a pulse from the ten to hundreds of nanoseconds, PFLs can range from several feet to several dozen feet in length depending on the dielectric used. These dielectrics also serve the dual purpose of providing voltage hold-off between conductors, and consequently are also used inside of the Marx itself. As a result of the insulating media and the large capacitance necessary to rapidly charge the transmission line, the system becomes extraordinarily bulky and difficult to calibrate and control.

Timing, high repeatability rate, enhanced controller capabilities and ease of use are extremely important for radiography applications. To accomplish this, a generator is needed that not only satisfies the above criteria, but also has integrated controls that incorporate some programmability.

APELC has developed an integrated Marx generator and on-board controller that fulfills such criteria. The MG15-3C-940PF (shown in Fig. 4.1) is a 15-stage, single-rail Marx generator. The device uses ceramic capacitors for energy storage and an acrylic liner for voltage hold-off. It can be charged from 10 to 40 kV, delivering a maximum output voltage of approximately 300 kV onto a 50-ohm matched load. The electrical specifications of this Marx generator are listed in Table 4.1.

This specific Marx generator is capable of delivering fast rise times (800 ps to 5 ns), moderate pulse widths (on the order of 25 ns), and can be operated with repetition rates (>100 Hz) for short durations. Our dynamic experiments are on the order of tens of microseconds in duration, and for these conditions the Marx banks are fired in single-pulse operation. In general, the addition of inductive charging elements to the Marx system yields a generator that is stable, low-impedance, and compact in its construction. This low-energy generator is ideal for soft x-ray applications requiring 300 kV, fast rise, short duration pulse or multi-pulse sequences.

APELC is currently working in the fabrication and assembly of two Marx generators for the NNSS Source Development project. The Marx generators will then be coupled to the multi-pulsed adder for x-ray diode testing at NNSS TDI later in 2021.

Figure 4.1. Top: A 15-stage, 300 keV Marx generator (APELC).
Bottom: Physical dimensions of the MG15-3C-940PF Marx generator.

Table 4.1. Electrical specifications of the MG15-3C-940PF Marx generator.

Parameter	Description	Value	Unit
V_{open}	Open circuit voltage	600	kV
V_{ch}	Maximum charge voltage	40	kV
N	Number of stages	15	--
N_{cap}	Number of capacitors per stage	3	--
C_{stage}	Capacitance per stage	2.82	nF
C_{marx}	Erected capacitance	188	pF
L_{marx}	Erected series inductance	526	nH
Z_{marx}	Marx impedance	53	Ohm
EFF_{volt}	Voltage efficiency into 50 Ohm load	48	%
P_{power}	Peak power	950	MW
E_{marx}	Energy stored in Marx	33	J
T_{ch}^{*}	Time to charge	2	ms
T_{RR}^{*}	Maximum repetition rate	200	Hz
P_{ave}^{*}	Average power	6600	J/s

4.2.2. Multi-pulse adder

Traditional multi-pulse systems require multiple uncoupled sources, each driving a unique load. However, by using injection wave generator (IGW) technology, coupling multiple sources to a single load transmission line can be achieved. Therefore, multiple sources can drive a single load element.

APELC uses two technologies in their multi-pulse adder design, the first of which is IGW, which demonstrates the ability to add multiple electrical pulses from unique sources onto a common output transmission line. The second technology, the wave-erection Marx generator, offers extremely fast-rising, high-voltage, short-duration pulses. It is from these two technologies that the multi-pulse adder was developed and demonstrated [10, 11].

In the multi-pulse adder design, each generator is essentially isolated from the common transmission line with magnetic material, as shown in Fig. 4.2. Also, all of the injection points are located at a common point on the output transmission line. Essentially, when the system is fired each generator delivers a pulse onto the common transmission line. The forward-moving wave proceeds directly to the load and the rearward-moving wave is launched toward the short of the common transmission line. However, upon reflection, most of the energy of the rearward-moving wave is absorbed back into the magnetic material, resetting the ferrite to its original state.

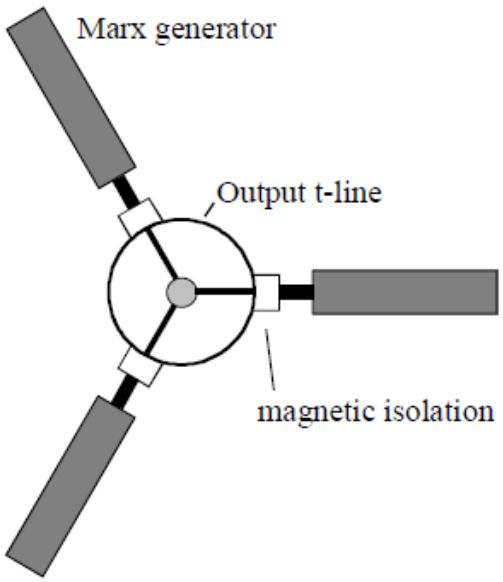

Figure 4.2. Illustration of a generator interconnection with output transmission line.

The pulse magnitudes produced by the system are on the order of several hundred kilovolts, with a pulse separation of tens of nanoseconds or microseconds.

In FY 2020, APELC designed and built a multi-pulse adder to be integrated and utilized with Wolfsbane soft x-ray system. The adder was preliminarily tested with low-voltage inputs for basic electrical performance characteristics with a time-domain reflectometer and a delay generator. Fig. 4.3 provides photographs of the adder. The adder body was designed for up to three coaxial inputs based on the Dielectric Sciences 2077 high-voltage cable with APELC's quick disconnect connectors.

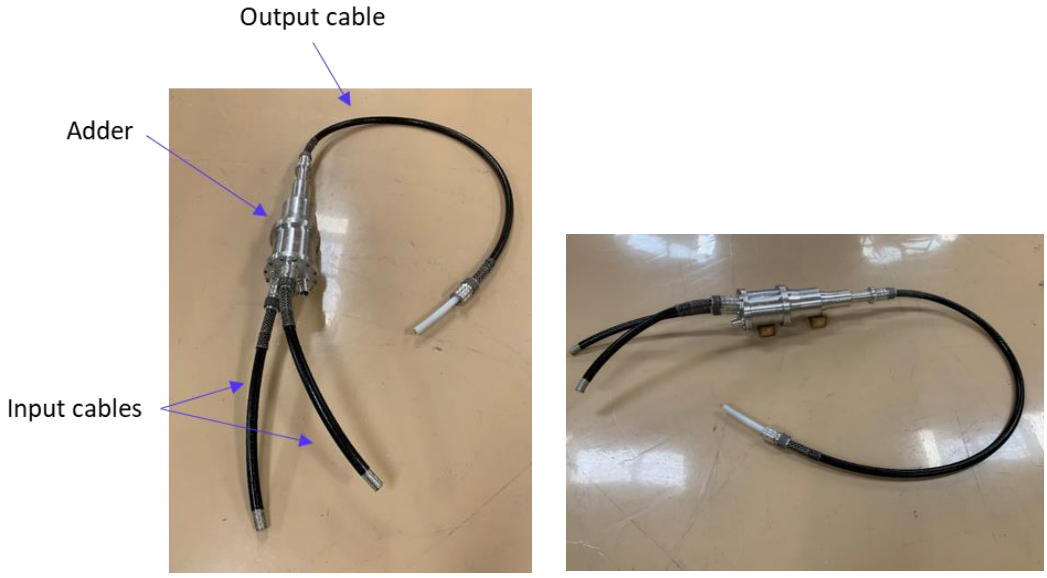

Figure 4.3. Photographs of the adder and coaxial cable connections.

A time domain reflectometer (TDR) was used to understand the impedance characteristics through the adder. The adder represents a high impedance, which helps isolate multiple inputs. As shown in Fig. 4.4, the source cable has a 70-ohm impedance. The adder section has an impedance of approximately 125 ohms, with an electrical length of approximately 3 ns.

A Stanford delay generator, with clean electrical pulses at lower voltage than the Marx generators, was used to drive both inputs of the adder. Fig. 4.5 shows the output of the adder. For lengthy pulses, the results are very good. Fig. 4.6 provides a zoomed-in view of the rising edge of the first pulse. As expected, there is some loss in amplitude due to the impedance mismatches, as the pulses propagate through the adder structure. The initial portion of the pulse from the delay generator is very close to a short Marx pulse, which is approximately half the peak voltage.

The next steps are to use Marx generators to source the adder and to fully characterize the system.

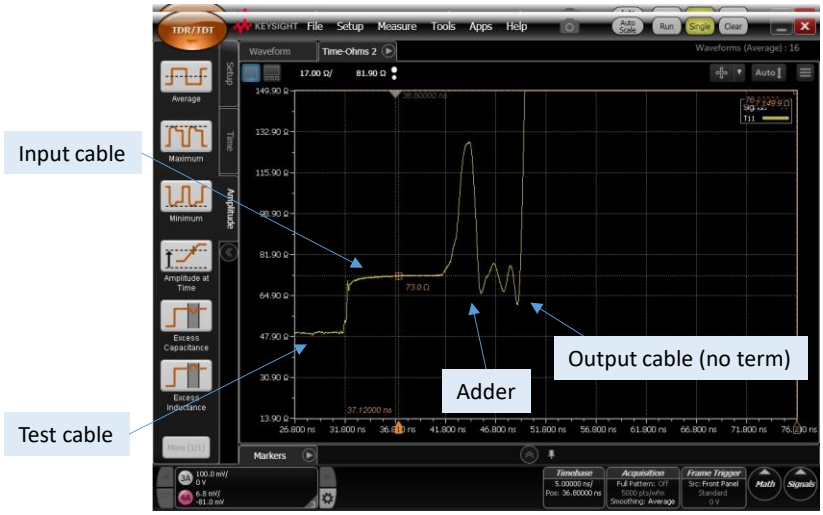

Figure 4.4. A TDR measurement on the adder showing combined output signals.

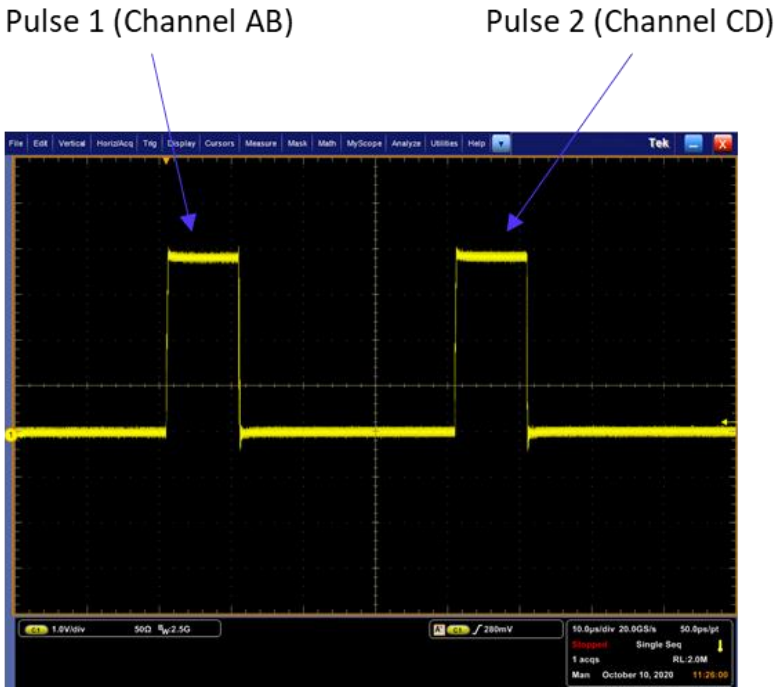

Figure 4.5. A two-pulse low-voltage measurement of output through the adder.

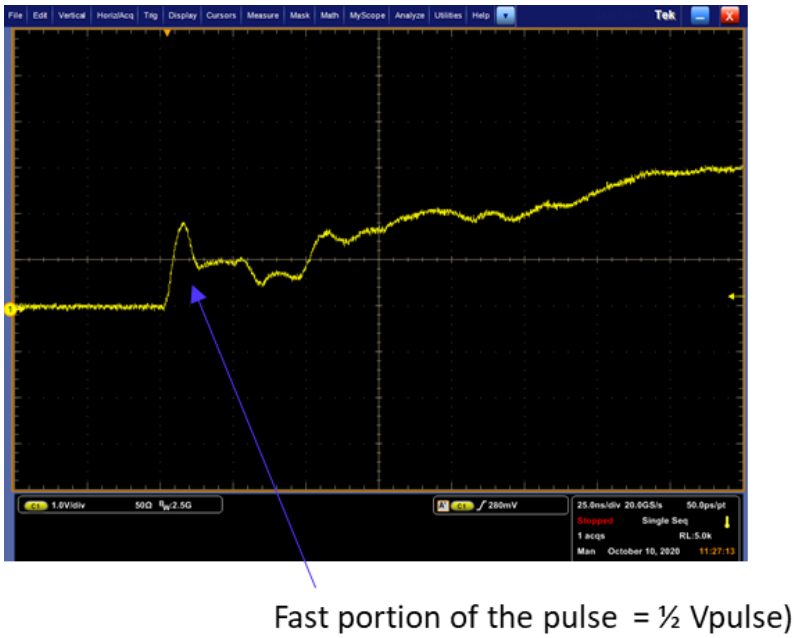

Figure 4.6. The two-pulse measurement, zoomed-in on the rising edge of the first pulse.

4.3. Imaging detector - Kraken digital framing camera

High-speed imaging is a core diagnostic capability for NNSS. Experiments that provide essential data for the stockpile mission generally involve measurements on the behavior of materials under extreme conditions. Materials that are shocked under an HE drive, as in subcritical experiments such as Wolfsbane, exhibit behavior that changes over very rapid timescales measured in millionths or even billionths of a second. Characterizing and understanding this behavior requires radiographic and/or optical imaging to track motion on these timescales. Framing cameras provide a discrete series of images over a short period of time with individual inter-frame times that must be extremely short in order to capture fixed-frame images of rapidly evolving phenomena such as HE shock-driven ejecta, dynamic compression of metals, and high-velocity fluid flow.

The Kraken framing camera is an imaging system capable of taking eight frames of images at a 10 MHz frame rate [12]. The system uses a CMOS readout integrated circuit bonded with a silicon detector, with an active area of 24 by 24 mm, resolution from an 800 by 800 pixel array, and a 30 µm pixel width. The sensor, BBAR VIS coated >90% transmission, is a 12-bit monochrome detector (Fig. 4.7). The camera supports an integration time minimum of 50 ns, and an interframe time minimum of 50 ns. Furthermore, the flexible camera system architecture will allow us to integrate a tiled four-sensor imager into future cameras for higher-resolution applications. The tiled

Kraken camera system will be a 49 × 49 mm (70 mm diagonal) active area imager with a resolution of 1600 by 1600 pixels. The four-sensor, four-control board system will be capable of capturing 8 frames at 70 mm or 32 frames with 35 mm offsets (Fig. 4.8).

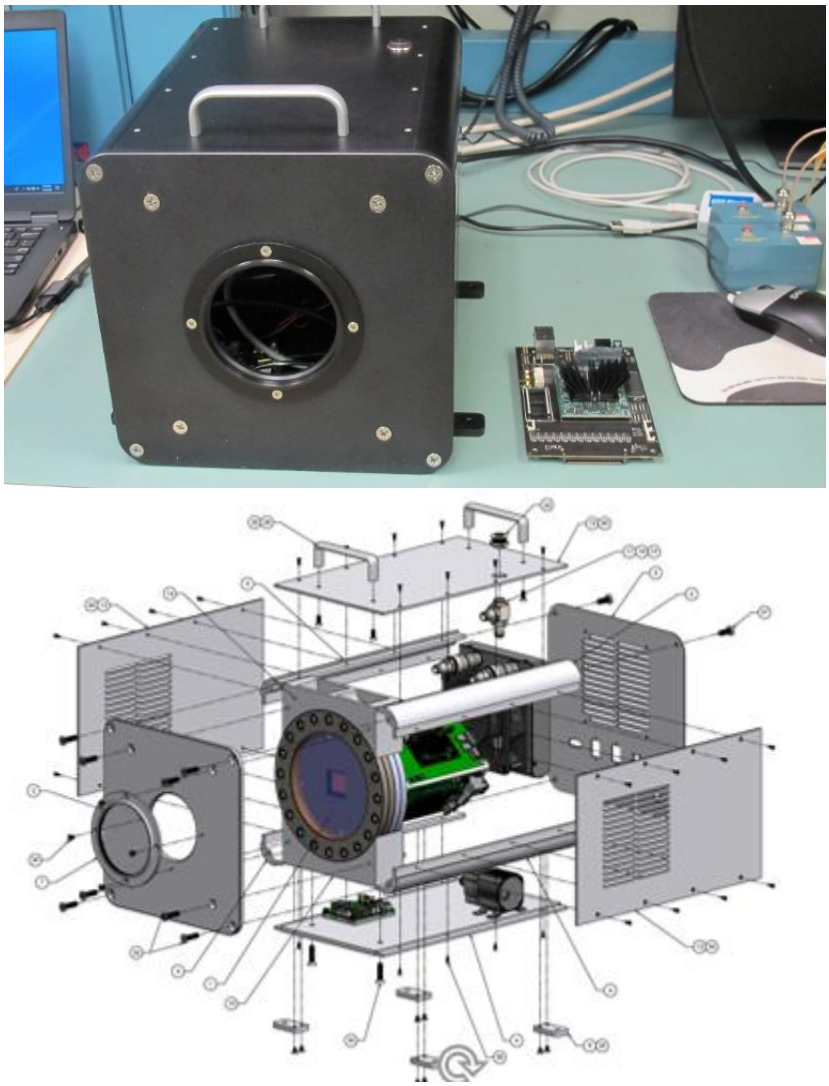

Figure 4.7. Top: Single-sensor Kraken camera system with new logic board. Bottom: Exploded view of single-sensor Kraken camera.

Kraken is software controlled using a PC over Ethernet. The images are read out as 16-bit raw image files in the TIFF format. The user interface embraces a simplified design to ensure intuitive operation. As many configuration settings as possible are automated. The interface supports concurrent software and hardware arming and triggering through on-screen buttons or BNC cables (Fig. 4.9).

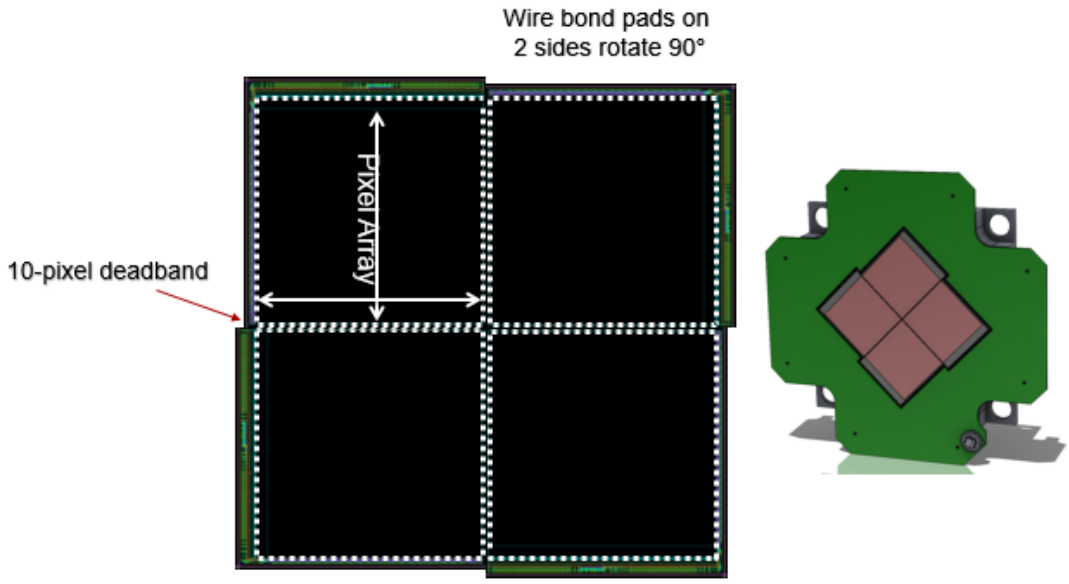

Figure 4.8. Tiled Kraken sensor (1600×1600 pixels) for future large-area imager camera system.

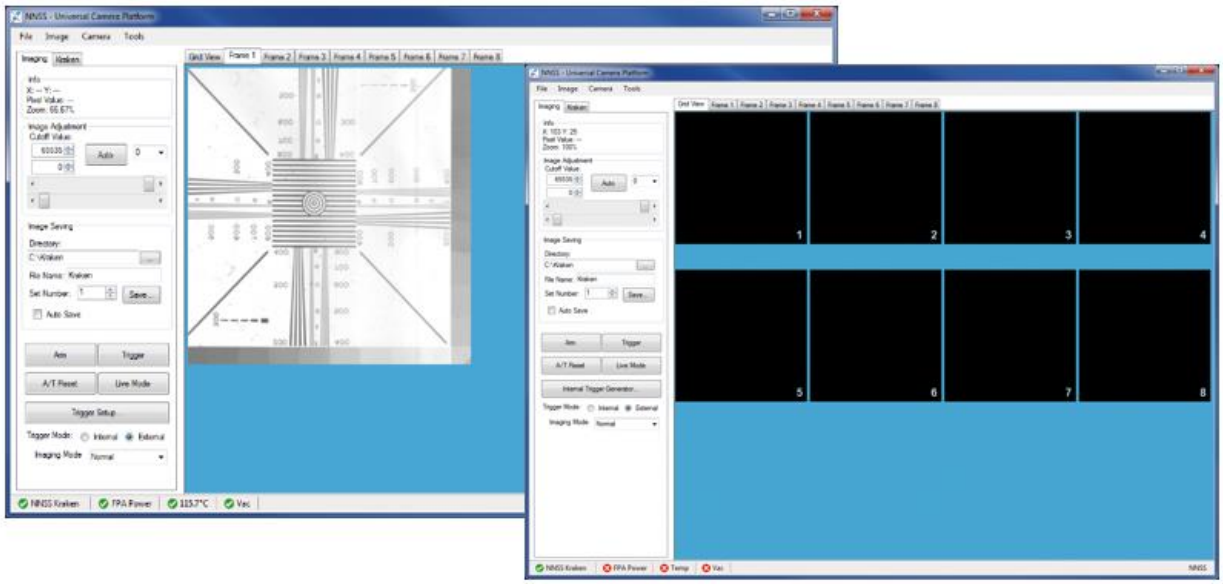

Figure 4.9. Universal camera architecture (UCA) software uses one interface to control multiple cameras.

The Kraken camera enclosure is designed with several ease-of-use features. The camera has swappable mounting feet, selectable for either SAE or metric table compatibility, that allow a user to mount it directly to an optical table. Optical center can either be set between optical mounting rows or in line with optical mounting rows. The camera lens mounting system is swappable for any type of lens mounting system

up to M-95 format lenses. The entire front plate of the camera can also be safely removed to minimize distance to the focal plane array should the need arise for use with custom optical image relay lens systems.

The Kraken camera system has several advantages over earlier electro-static image tube–based framing cameras. As a fully contained plug-and-play system, the camera does not need any external power supplies beyond the included AC adapter brick. The cooling system is built into the camera, so no external circulators or chillers are required. Compared to tube-based cameras, the Kraken's silicon sensor provides higher overall sensitivity without any distortion or blur. The large optical opening provides ample flexibility for various optical relays. The end user needs to supply facility 15 A power, a PC with the Kraken operating software, and optional arm and trigger source signals.

A recent sample of shadowgraphy images obtained with the Kraken camera are shown in Fig. 4.10.

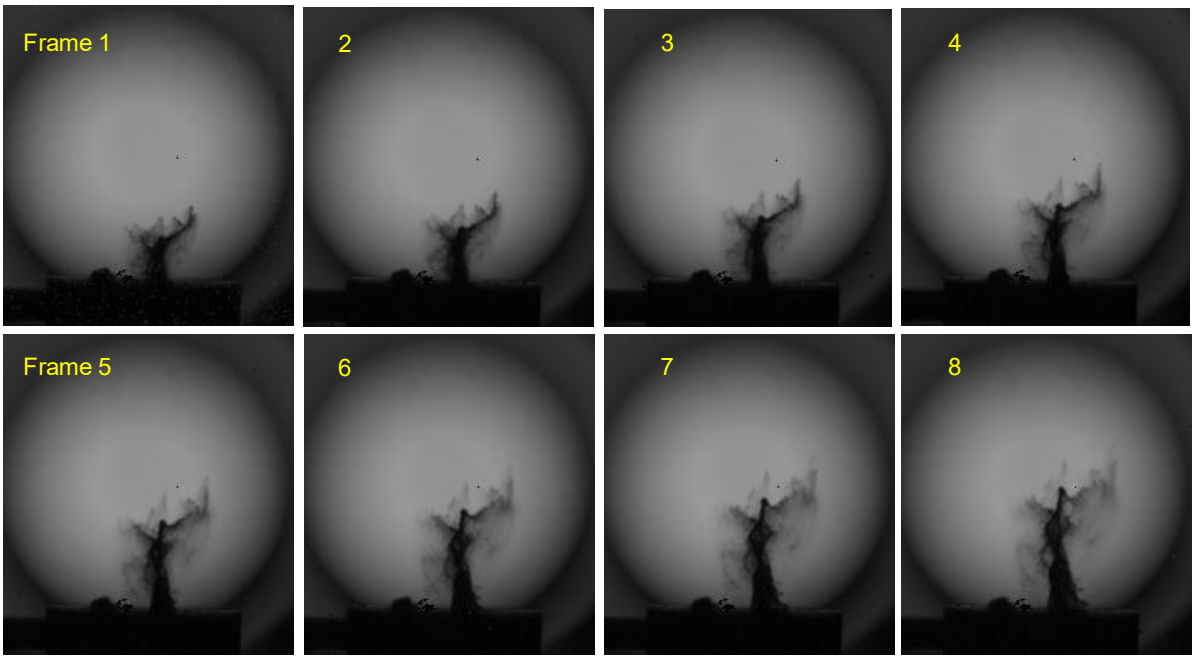

Figure 4.10. Ejecta shadowgraphy dynamic test performed at NNSS TDI in Los Alamos. This image captures laser-driven ejecta with the Kraken, digital 8-frame camera. A high-powered laser provides a shock impulse to a packet of 5 to 30 µm silica spheres staged at the bottom of the scene. The laser impact sends the particles up into the field of view recorded in an eight-frame time sequence on the Kraken camera. An LED backlighter is used to illuminate the shadowgraph images for the camera.

4.4. Two-wavelength shadowgraphy

NNSS has proposed the development of a new multi-frame, two-wavelength shadowgraphy diagnostic to characterize ejecta on future Red Sage–type experiments. The diagnostic will be used to provide spatially and temporally resolved images of ejecta emitted from a shocked surface utilizing a light source at two different wavelengths. Up to 16 images will be acquired using a newly developed high-speed framing camera (Kraken). The light source is under development. The data will provide qualitative spatially and temporally resolved information about the evolution of an ejecta cloud. In addition, with the multiple wavelengths and an areal density measurement, the average particle size can be estimated with much smaller uncertainty than previously possible. A two-wavelength, single-frame system has been developed to evaluate the diagnostic and to determine to what level of accuracy an average particle size can be extracted from the shadowgraphy images.

The following paragraphs describe work performed in FY 2020; future plans are also included.

4.4.1 Past shadowgraphy work

Visible shadowgraphy/imaging has been used in a variety of applications over the years to observe ejecta particles emitted from shock-loaded samples. The diagnostic provides excellent qualitative information about the spatial and temporal evolution of an ejecta cloud. In addition, these data can be used to determine if some aspects of the physics experiment are performing as expected. The diagnostic was successfully implemented on a number or HE cylinder experiments at LANL firing sites over the past many years. With excellent results on several local tests the diagnostic was carried forward to SCEs on Thoroughbred (2000), Barolo (2009), and Lyra (2018).

In some cases, the shadowgraphy images, or single detector measurements along with areal density measurements, have been used to estimate the average particle size. If Mie theory is applied to the shadowgraphy images along with a measurement of the ejecta areal density, an estimate of the average ejecta particle size can be determined. This analysis approach was applied to the Lawrence Livermore National Laboratory (LLNL) subcritical experiment Piano [13, 14] using a single detector and single wavelength. The diagnostic was called the average particle diameter diagnostic (APDD). A similar analysis approach was applied to Barolo shadowgraphy images to constrain the average particle size [15]. In these cases, an average particle size was derived, but with relatively large uncertainty. Recently, it was proposed by LANL and

NNSS to extend the shadowgraphy diagnostic technique by acquiring shadowgraphs at two different wavelengths [16]. By using two wavelengths the particle size can be further constrained.

4.4.2 Experimental layout for dynamic tests

A simplified shadowgraphy system was developed and implemented to conduct a two-wavelength shadowgraphy dynamic ejecta test in the lab at TDI. In order to avoid the use of an HE drive, a high-power laser provided a shock source. The Ekspla (532 nm) class IV laser is capable of producing 120 ps pulses. As applied to the ejecta test, the laser's horizontally emitted beam is redirected to a vertical position (using a 45° turning mirror) where it produces an indentation/ablation onto a thin glass/copper tape target platform (Fig. 4.11).

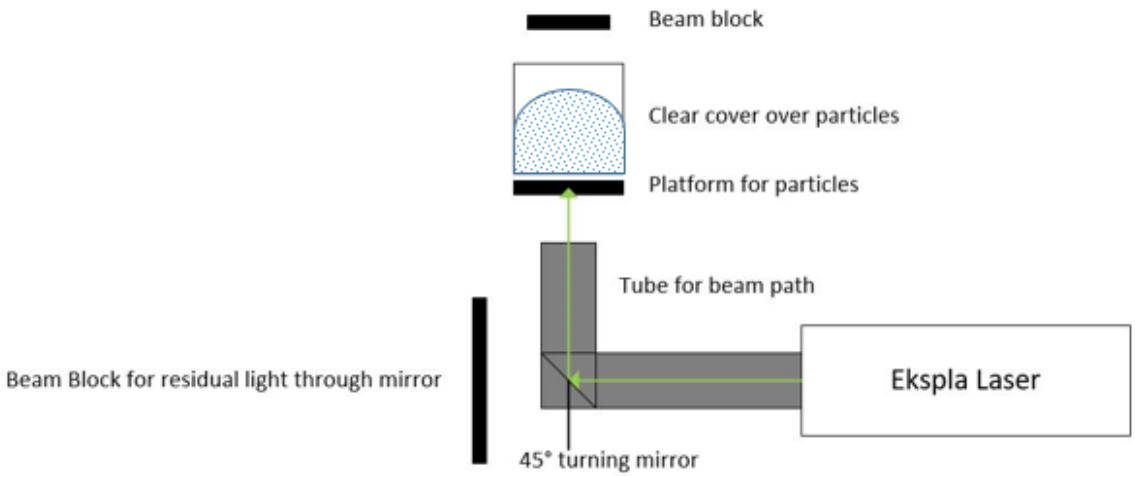

Figure 4.11. Side view (not to scale) of ejecta test layout; cameras and dual wavelength light source are not shown.

The target platform contains a packet of particles with a predetermined mass and known particle diameter distribution. When the incoming laser beam hits the target, the shocked surface sends the particle cloud up into a field of view where the data are recorded using two cameras for two LED light sources operating at different wavelengths (Fig. 4.12).

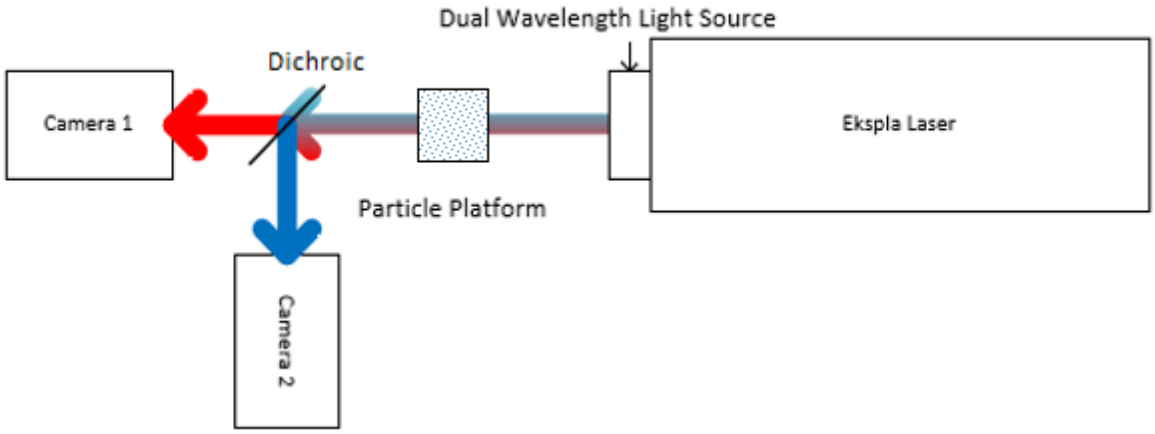

Figure 4.12. Top view of Imaging setup.

The dual-wavelength light source used in this experiment is a Lumiled LED capable of operating at 415 nm (blue) and 660 nm (red) wavelengths, respectively. Two PiMAx4 cameras were used for single image acquisition (one for each wavelength). The cameras have an active sensor area of 13 × 13 mm with a 1024 × 1024 pixel array (12.8 μm/pixel).

In order to get the initial timing from laser pulse to camera exposure, aluminum shavings were used; the aluminum shavings size related well to the camera pixels. Once timing was fine-tuned, different materials with known particle sizes were utilized for the dynamic tests including Alumina particles 300 nm in diameter and silica spheres ranging from 5 to 90 μm in diameter. The alternating blue/red LED source was used to back illuminate the particle cloud. Two pieces of opal glass and a 1 ND filter were placed in front of the light source so that the camera would not saturate. A dichroic was placed further down the line of sight to split the signal into two wavelengths so each camera only captured one color. A PiMax4 camera captured one image per wavelength path. The camera exposure was set to 130 ns and the light source was pulsed for 75 ns. The images in Figs. 4.13–4.16 show the results obtained using the two-wavelength shadowgraphy system.

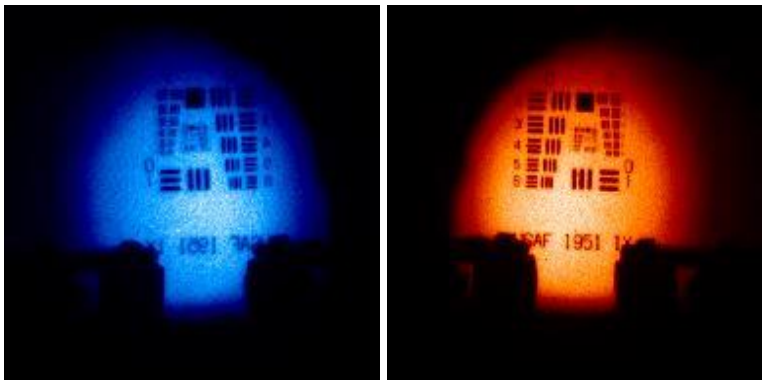

Figure 4.13. Camera focus for both wavelengths using Air Force target.

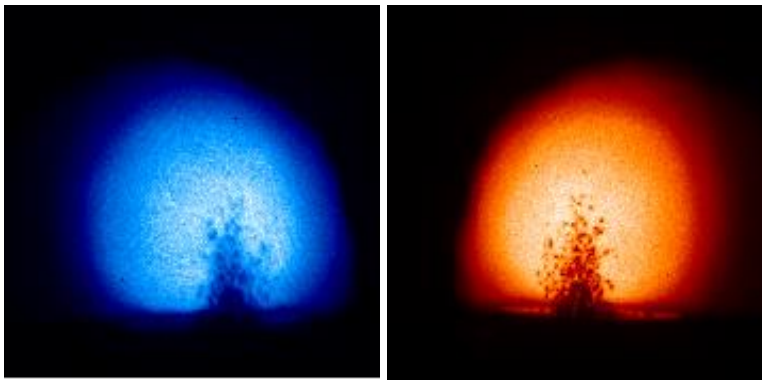

Figure 4.14. Aluminum shavings for timing.

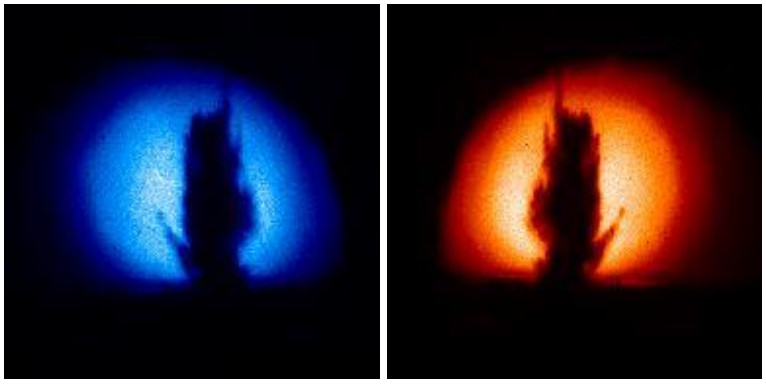

Figure 4.15. 300 nm alumina particles.

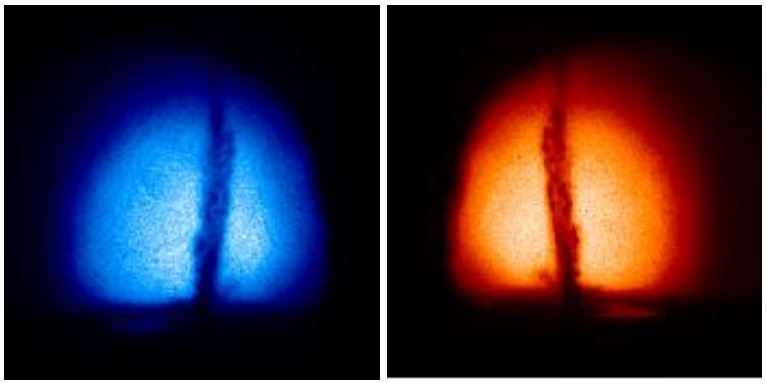

Figure 4.16 Silica spheres 5–90 µm in diameter.

As mentioned earlier, single-frame images were acquired for the dynamic test. The two-wavelength shadowgraphy system has been upgraded to include two digital 8-frame Kraken cameras (Fig. 4.17). Dynamic experiments will be conducted with the high-speed framing cameras to acquire eight images for each wavelength (415 nm and 660 nm).

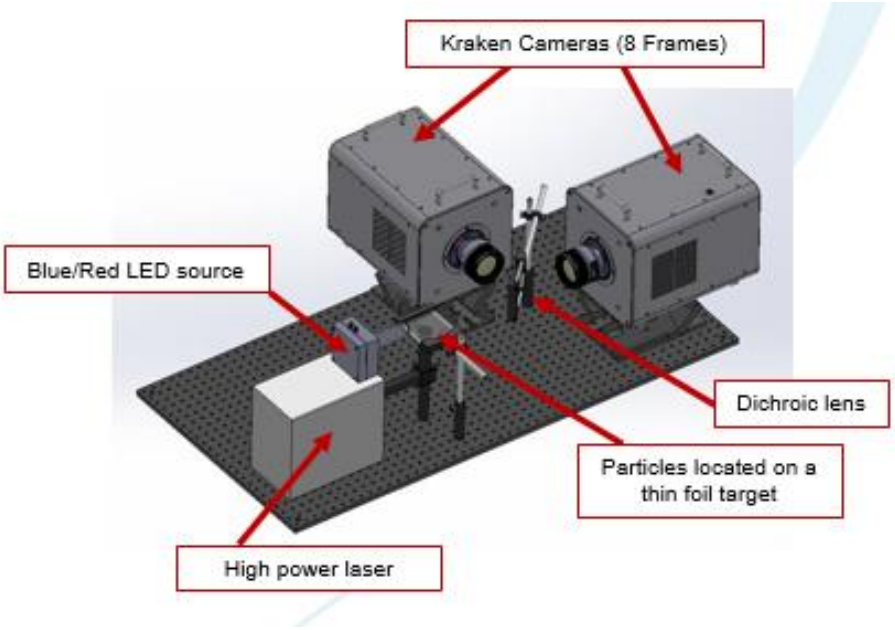

Figure 4.17. Laser-driven ejecta particle testing using two Kraken cameras.

4.4.3 Application of Mie theory

Small particles have much larger scattering cross sections at larger angles than larger particles. The theory used to describe light scattering from particles is Mie theory, and much of the derived equations below follow from the work in Ref. [6].

As an example of Mie theory, Fig. 4.18 shows the unpolarized irradiance vs. scattering angle for 0.5, 1.0, 5.0, and 10.0 μm diameter particles.

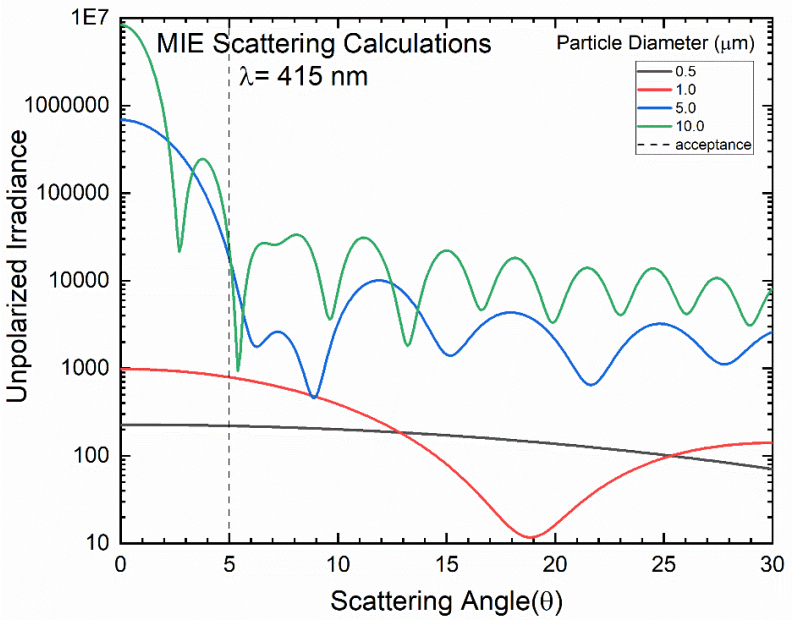

Figure 4.18. Mie scattering calculation of irradiance vs. scattering angle for SiO_2 particles. Calculations are presented for 0.5, 1.0, 5.0, and 10.0 μm diameter particles at a wavelength of 415 nm. The dashed line at 5 degrees is the acceptance of the optical relay system for data obtained at TDI in October 2020.

Fig. 4.18 illustrates that, for a given wavelength, large particles scatter light in the forward direction with a much higher cross section than smaller particles. The cross section differences make it impossible to determine from a shadowgraph (transmission measurement) what size particles are scattering the light. However, if x-ray radiography is performed at the same time that mass areal density is measured, then the following general statements can be made:

1. If the ejecta cloud is optically thin (high transmission), and radiographically thick, => large particles
2. If the ejecta cloud is optically thick (low transmission), and radiographically thin, => small particles

Fig. 4.19 shows scattering intensity calculations for a single size particle at two different wavelengths. These calculations indicate that if ratios of images are taken near zero degrees, variation from unity inform us about the particle size.

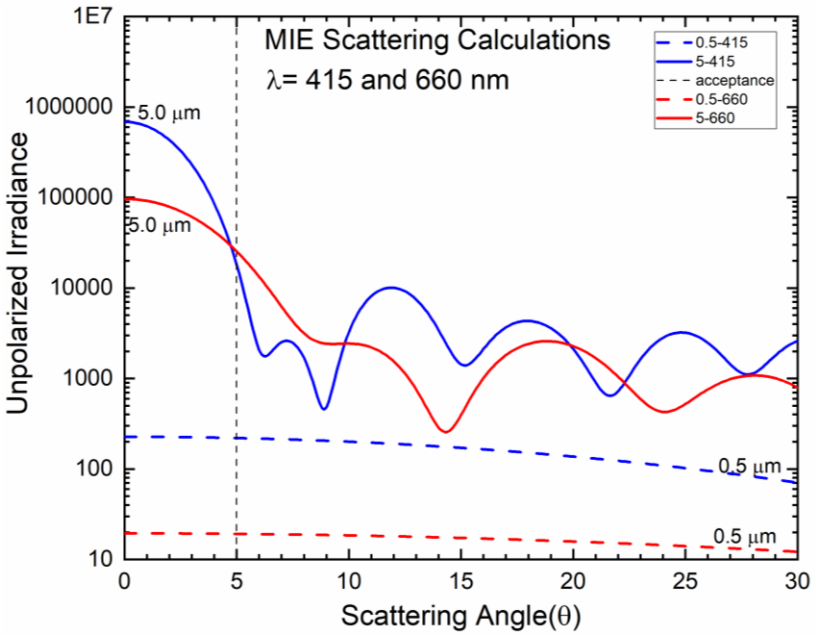

Figure 4.19. Mie scattering intensity calculations at two different wavelengths of 415 nm (blue curves) and 660 nm (red curves). Dashed curves are particles 0.5 μm in diameter, and the solid curves are particles at 5.0 μm in diameter.

4.4.4 Mie theory applied to transmission measurements

Following Ref. [6], an expression can be derived for the transmission of light through a cloud (or slab) of particles of thickness τ. The amount of light dI removed from the incident beam (along the z direction) of light by the cloud of particles between z and dz can be written as

$$dI = \alpha_{ext} I dz. \tag{1}$$

Integrating Eq. 1, we get

$$\mathrm{T} = \mathrm{e}^{-\alpha_{ext} \cdot \tau}, \tag{2}$$

where T is the transmission of light, and α_{ext} is the attenuation coefficient

$$\alpha_{ext} = \frac{dN}{dV} \int_0^\infty q_{ext}(r) \cdot \pi r^2 dr, \tag{3}$$

where $\frac{dN}{dV}$ is the distribution of particles per unit volume, q_{ext} is the Mie extinction coefficient, and r is the radius of the particle. In the following, $\frac{dN}{dV}$ is found by relating the parameter to the mass areal density as measured from the radiography. The mass areal density (σ) is simply

$$\sigma = \rho \cdot \tau \,, \tag{4}$$

where ρ is the mass volume density of the cloud of particles. The mass of the ith particle (m_i) is

$$m_i = \frac{4}{3}\pi {r_i}^3 \cdot \rho_p \,, \tag{5}$$

where ρ_p is the density of the particle, and r_i is the radius of the ith particle.

Therefore, the particle number distribution can be related to the mass areal density as

$$\frac{dN}{dV} = \frac{\sigma \cdot \tau}{\frac{4}{3}\pi r^3 \rho_p} \,. \tag{6}$$

Finally, Eq. 2 can be rewritten as

$$\frac{q_{ext}}{D} = \frac{2 \cdot \rho_p \ln(T)}{3\sigma} \,, \tag{7}$$

where D is the particle diameter. This expression is given as it is presented in Ref. [11]. In practice, the right-hand side of the expression is solved using the experimental data for the optical transmission (T), and the mass areal density (σ) from the x-ray radiography. The particle diameter can then be obtained from a plot of the left-hand side of the expression. Fig. 4.20 shows an example of the left-hand side of the expression for SiO_2 particles. The figure shows two plots for two different wavelengths. For a single wavelength there can be some ambiguity as two particle diameters can correspond to the same value of the left-hand side of Eq. 7. With two wavelengths however, this ambiguity is removed, and provides a tighter constraint on the particle size.

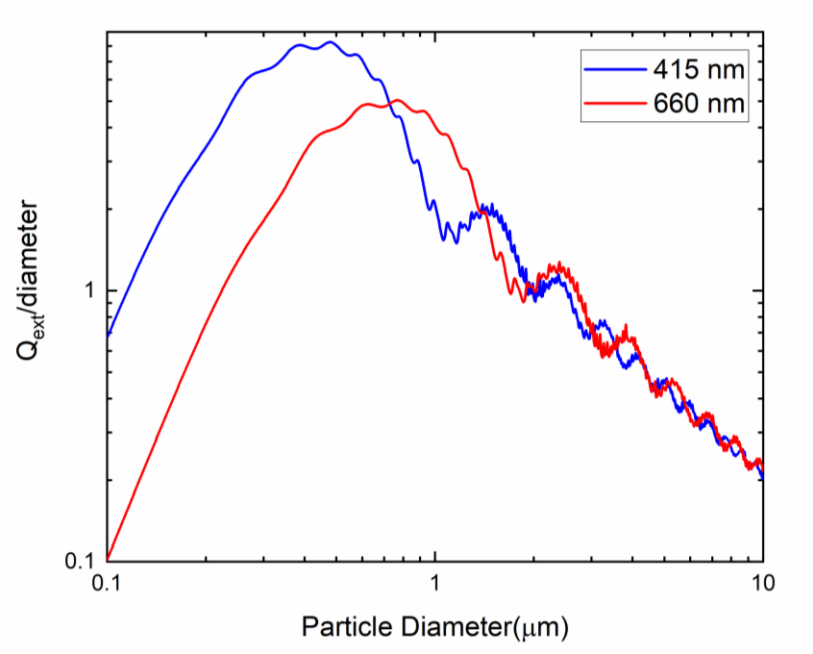

Figure 4.20. Calculated Q_{ext}/particle diameter for the two wavelengths of 415 nm (blue curve) and 660 nm (red curve). Mie calculations were performed for SiO_2 particles.

Shadowgraphy has been used successfully in the past to provide unique spatially and temporally resolved images of ejecta after being emitted from a shocked surface. For many of the past experimental measurements, a white light strobe was used, so a broad band of wavelengths were present, making it difficult to determine particle sizes. By going to single wavelengths for illumination, and using two wavelengths, the shadowgraphs will not only give valuable qualitative information about the dynamics of the ejecta, but provide the ability to extract particle size using Mie theory as described above.

5. INTEGRATED DIAGNOSTIC DESIGN CONCEPT

A conceptual multi-probe diagnostic has been developed to understand ejecta physics in the Wolfsbane series of subcritical experiments. The system was designed utilizing the Nightshade package as an initial physics model. The physics package is assumed to be contained in a six-foot vessel and the diagnostics to be integrated on the vessel's windows in such a way they will capture the relevant ejecta data on the same line of sight. The soft x-ray source consists of six Marx generators, two pulse adders and two diode heads (Fig 5.1). The diode heads were designed to reside inside the vessel and to cover the field of view of the top and bottom targets in the package (Fig. 5.2).

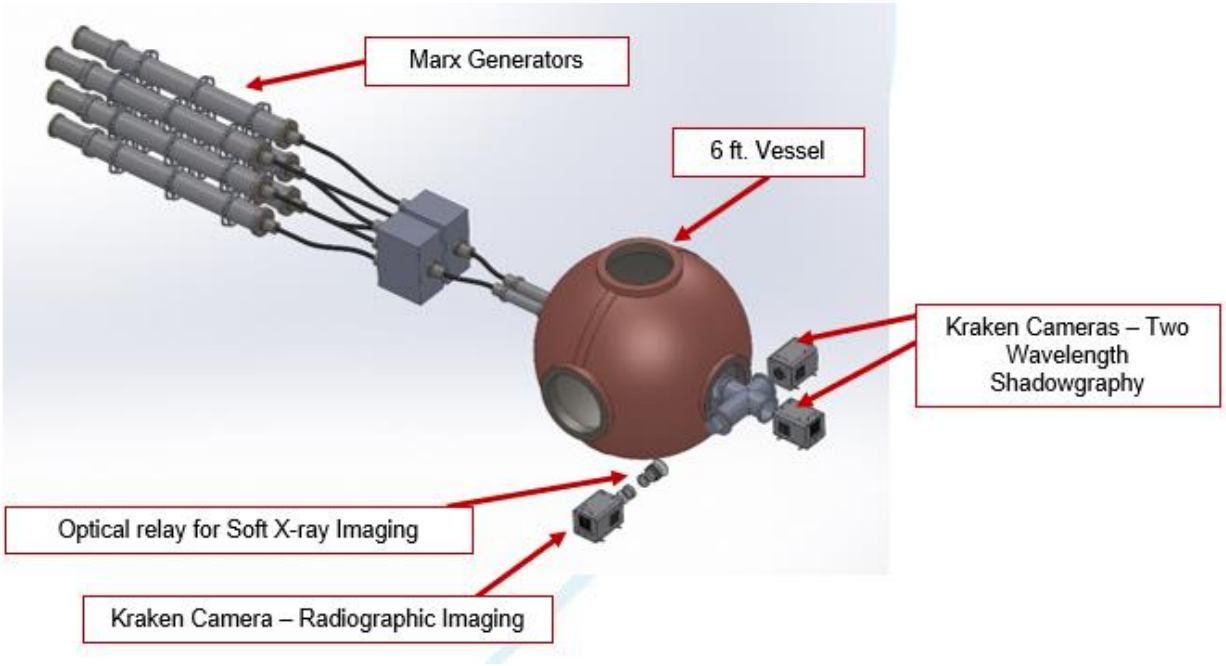

Figure 5.1. Conceptual multi-probe diagnostic for Wolfsbane (x-ray and shadowgraphy imaging).

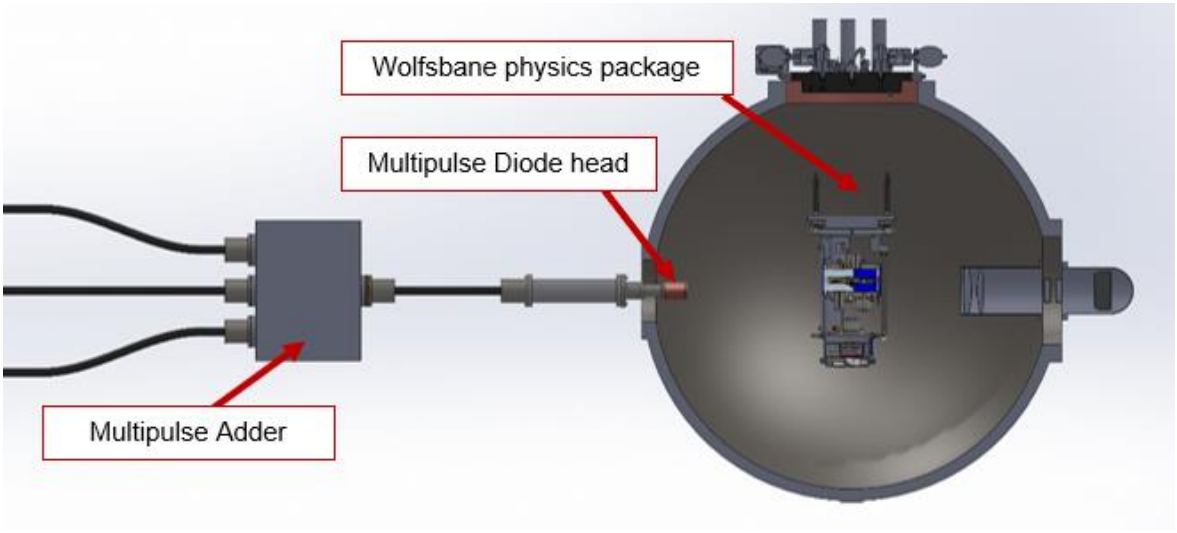

Figure 5.2. Conceptual x-ray source and imaging for Wolfsbane.

When combining x-ray and shadowgraphy imaging within the same optical relay system, it is required that the sources of light will be collected from different object distances. The shadowgraphy imaging has to see inside the packages; whereas, the x-ray imaging has a further standoff from packages, as Fig. 5.3 shows. The two shadowgraphy turning mirrors and the x-ray scintillators are mounted onto the experimental package.

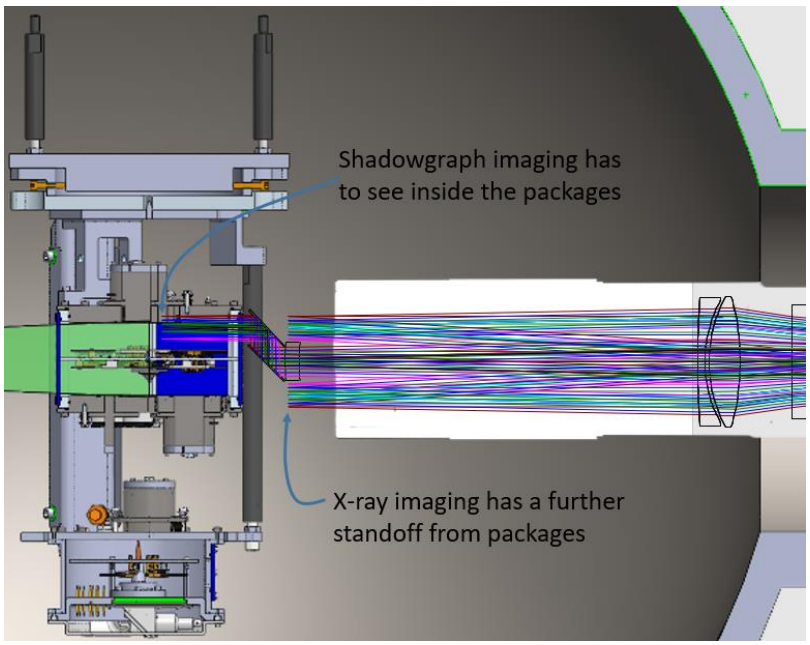

Figure 5.3. X-ray and shadowgraphy imaging conceptual layout.

The attempt is made to locate the vessel relay lenses close to the exit port to minimize clearance issues that may occur when moving the experimental package in or out of the confinement vessel.

Confinement windows have been positioned at the exit port of the vessel as well as at the exit port of the add-on vessel extension (double confinement window concept).

The complete imaging systems are shown below in Fig. 5.4. (The pellicle is rotated incorrectly in this view.) The system with only blue rays is for the blue LED shadowgraphy imaging. The system with only red rays is for the red LED shadowgraphy imaging. The center imaging system can record both x-ray and shadowgraph images.

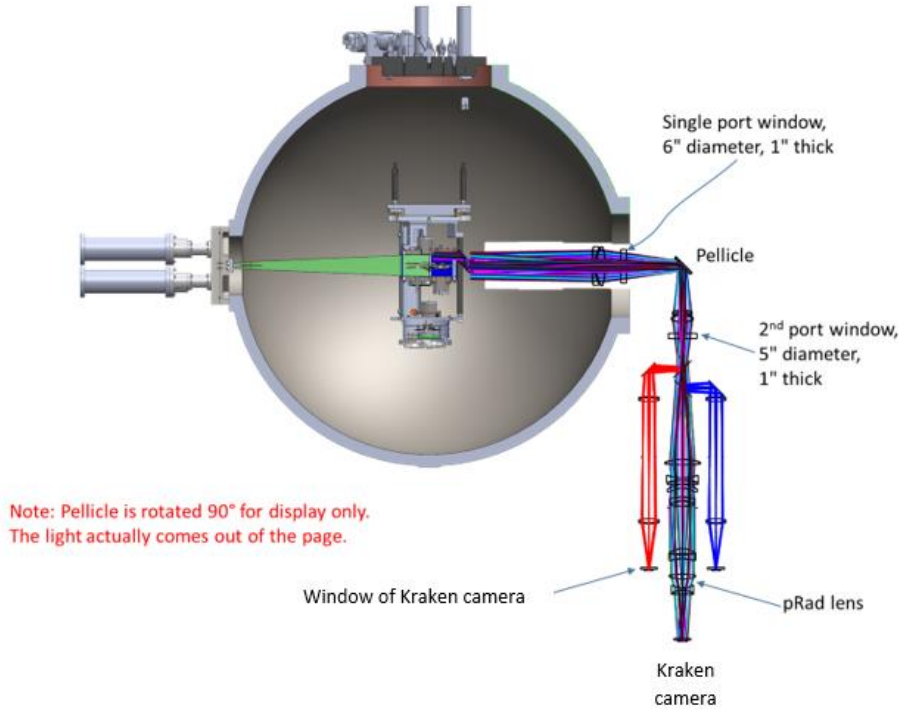

Fig. 5.4. Conceptual x-ray and shadowgraphy imaging systems ray trace.

In order for multiplexing shadowgraphy and x-ray imaging systems to operate along the same line of sight, three extra lenses are needed for the shadowgraph relay. The shadowgraph imaging path has to start 228 mm (estimate) before the x-ray scintillator plane. To compensate for this added object distance, one shadowgraph relay lens is placed between the gap in the x-ray scintillators, a second relay lens at the intermediate image plane of the x-ray imaging, and a third lens at the final CCD camera entrance window.

5.1. Radiography with shadowgraphy optical image relay system

The doublet shadowgraphy relay optics (placed after the beam splitters) are commercial-off-the-shelf units that are readily available (Fig. 5.5). For the current configuration, it was assumed that the shadowgraphy imaging will use two Kraken cameras, and the x-ray imaging will use the one Kraken camera.

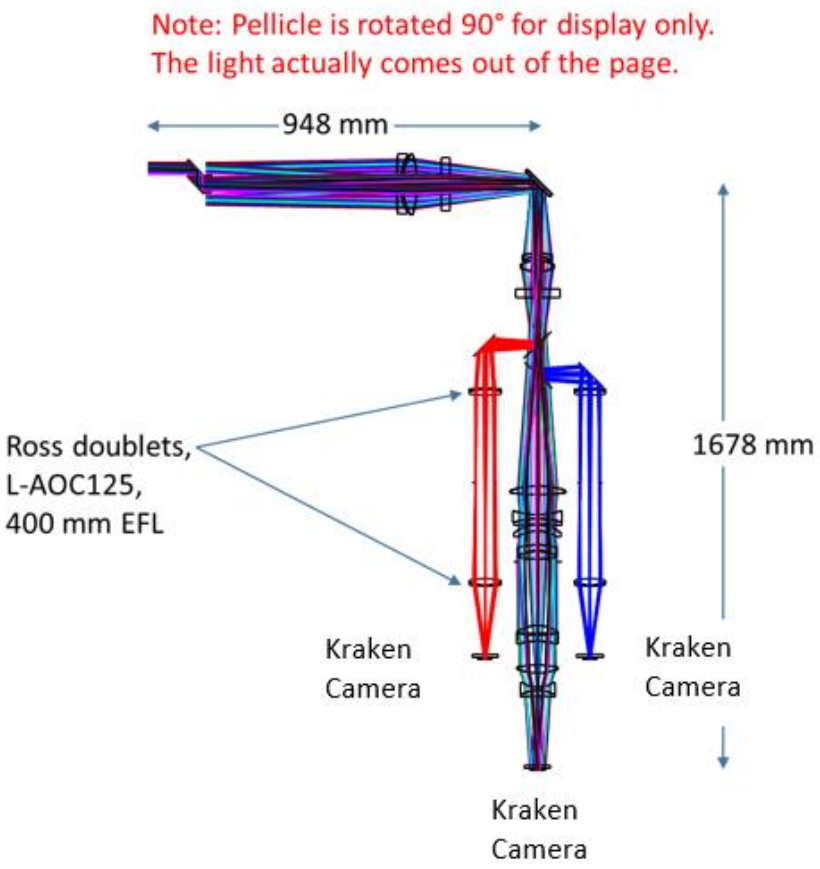

Figure 5.5. Conceptual optical relay systems for both x-ray and shadowgraphy imaging.

Figs. 5.6 and 5.7 show the relative positions of the rectangular shadowgraph lens and the x-ray scintillators. In Fig. 5.6, the upper ray trace is side view and the lower is a top-down view.

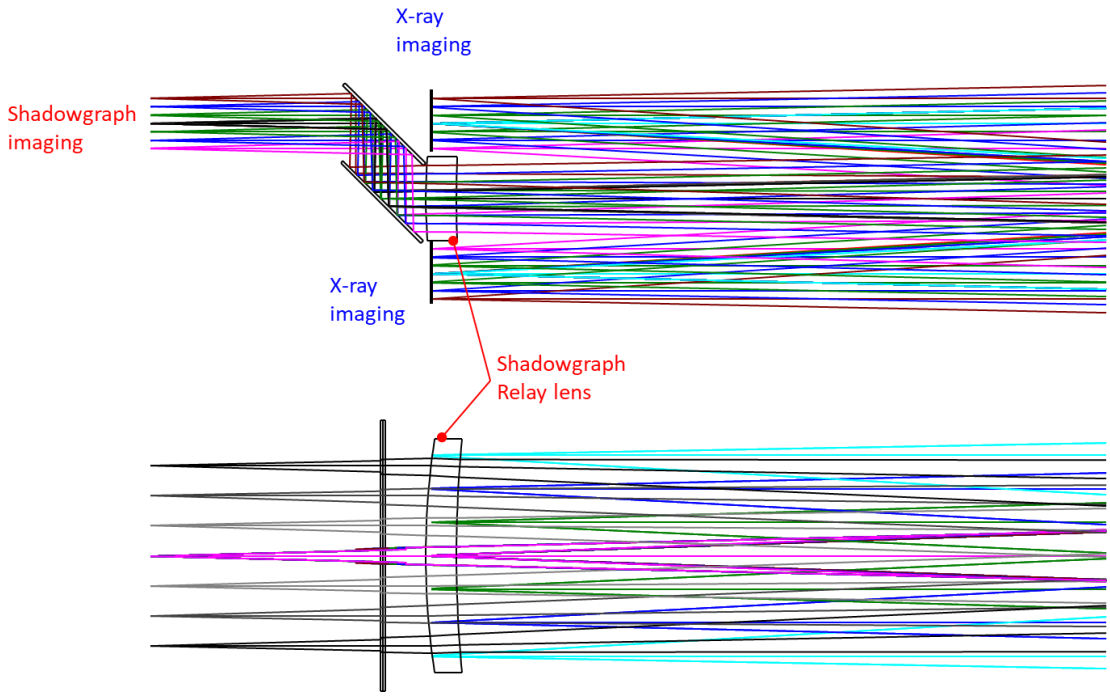

Figure 5.6. Rectangular lens utilized for shadowgraphy relay system.

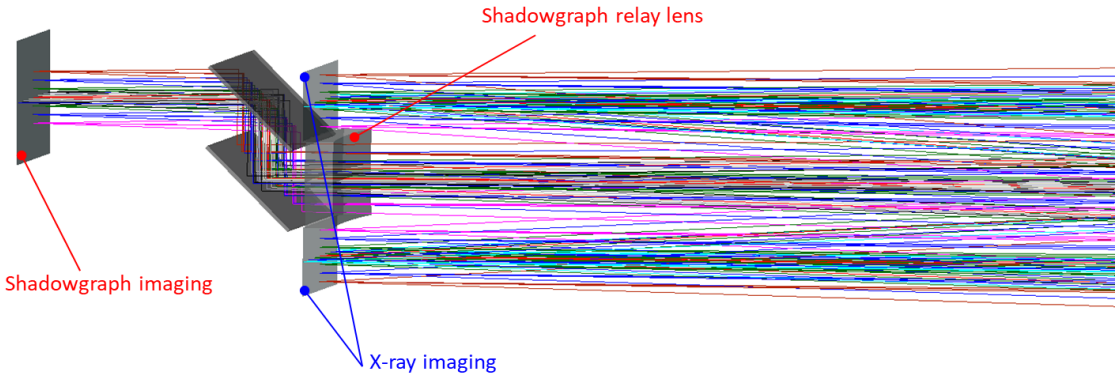

Figure 5.7. 3-D perspective view of scintillators for x-ray imaging and shadowgraphy relay system.

At the intermediate image location, the shadowgraphy and the x-ray intermediate images are at different distances along the optical axis. A rectangular lens is placed for the shadowgraphy imaging at the same plane as the x-ray imaging, where there are adequate clearances. This shadowgraphy lens compensates for the separation of the intermediate image planes. Fig. 5.8 shows both the *yz* and *xz* orientations at this intermediate plane location.

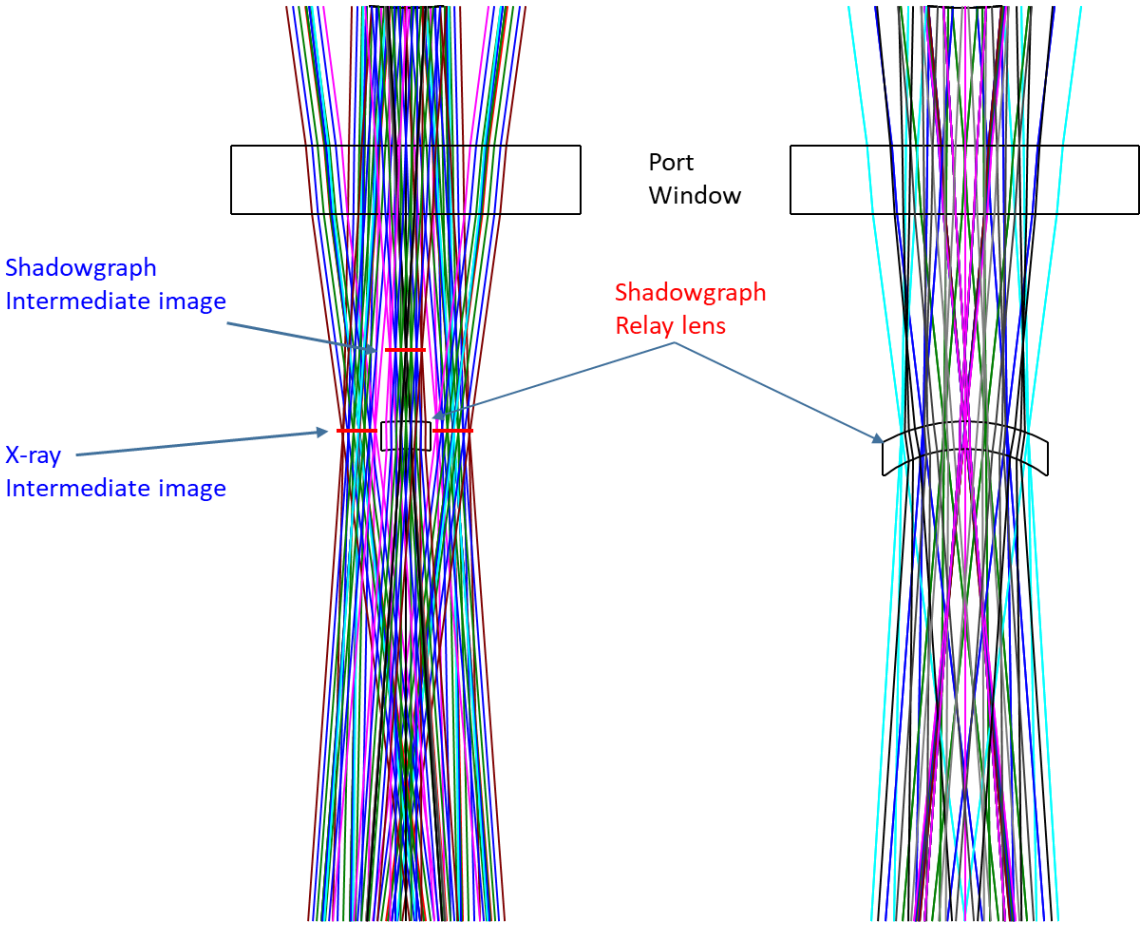

Figure 5.8. Intermediate image planes for both x-ray and shadowgraphy systems.

At the final image plane, a small rectangular lens is placed on the CCD window. This rectangular lens is used to place all image planes properly at the CCD. Fig. 5.9 shows both the *yz* and *xz* orientations at this location for the Kraken camera.

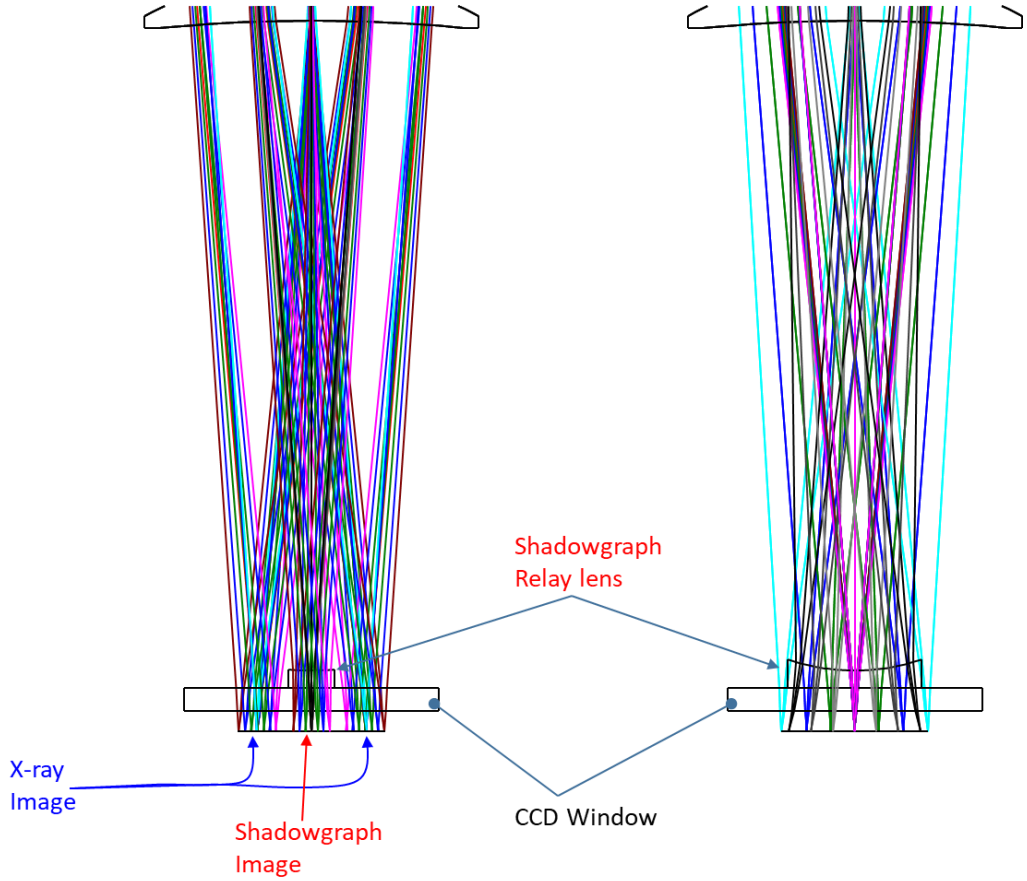

Figure 5.9. Image formation at the CCD plane (Kraken sensor)

Fig. 5.10 is a 3-D perspective view of the entire system with correct mirror orientations.

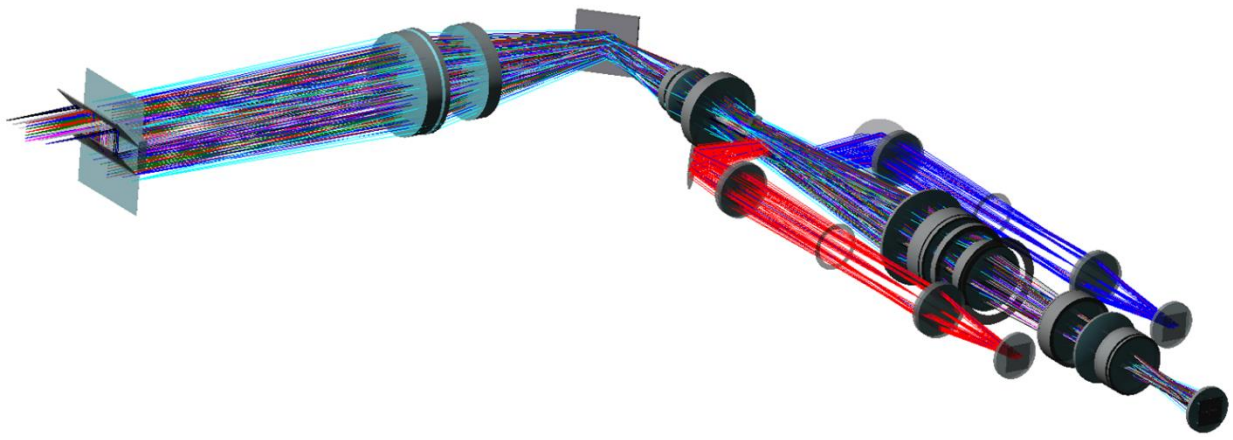

Figure 5.10. Optical systems for two-wavelength shadowgraphy and x-ray imaging.

6. CONCLUSION

In an effort to deliver better diagnostic information on the characteristics of double-shocked plutonium ejecta to LANL X-Division designers, the NNSS Advanced Diagnostics program has developed the experimental conceptual design described in this document, which will provide more complete ejecta density information along with a constraint on the size of the ejecta particles. This information will help LANL designers validate modeling codes of mix on converging systems.

Our proposed concept combines six-pulse soft x-ray radiography with two-color shadowgraphy over the same field of view and line of sight to add capacity for particle size evaluation. The single-anode multi-pulse soft x-ray source coupled with digital multi-frame Kraken imager recording will greatly enhance the thin material ejecta density measurement as well as providing more complete information on the evolution of the dynamic test. The two-wavelength multi-frame shadowgraphs synchronized with x-ray images will constrain the range of particle size in the ejecta cloud.

Additional work is needed to qualify performance of a six-pulse soft x-ray radiography system as well as the analysis techniques for the two-color shadowgraphy. Future scope will utilize the TDI laser-driven ejecta test bed for development of the two-color light source with multi-frame imaging. Multi-pulse soft source testing will also be carried out at TDI in the x-ray lab. Small-area Kraken cameras can supply high-quality imaging for shadowgraphy and a full-area Kraken will be needed for the large-area radiography images.

A challenge we must address is getting the source x-rays into the vessel. Our conceptual design is based on a six-foot vessel layout, which provides better access options than a three-foot layout would. Future efforts will pursue diagnostic qualification tests and designs for vessel configuration.

The Cygnus facility is scheduled to conduct Nightshade, Nimble, and Great Basin experiments through 2025. In the interim we will continue to develop this diagnostic and qualify it.

7. REFERENCES

[1] J. Danielson and A. Bauer. Nightshade Prototype Experiments – Silverleaf, LA-UR-16-27510 (2016).

[2] J. Danielson. Diagnostic Requirements for the Nightshade Series, LA-CP-19-20193 (2019).

[3] D. Phillips and D. Smalley. Presentation: Multi-Pulse Soft Radiography Development Progress (2017).

[4] M. R. Furlanetto. Report: Radiographic Options for Red Sage/Nightshade, LA-CP-15-00229 (2015).

[5] D. Sorenson. Presentation: Soft Radiography for Nightshade Soft Radiography (2018).

[6] C. F. Bohren and D. R. Huffman. Absorption and Scattering of Light by Small Particles (Wiley, New York, 1983).

[7] D. Platts, M. P. Hockaday, D. Beck, W. Coulter, and R. C. Smith. Compact Flash X-Ray Units. Proc. Tenth IEEE International Pulsed Power Conference (1995) 892-896.

[8] N. S. P. King, et al. Time Dependent Imaging of Cylindrical Shocks at the Pegasus Facility. Proc. Tenth IEEE International Pulsed Power Conference (1995) 1017-1023.

[9] D. V. Morgan, D. Macy, and G. Stevens. Real-Time X-Ray Diffraction Measurements of Shocked Polycrystalline Tin and Aluminum. Rev. Sci. Instrum. 79 (2008) 113904.

[10] J. R. Mayes, W. J. Carey, W. C. Nunnally and L. Altgilbers, "The Gatling Marx generator system." 28th IEEE International Conference on Plasma Science and 13th IEEE International Pulsed Power Conference, Las Vegas, Nevada, 2001, 468. 10.1109/PPPS.2001.961243.

[11] Mayes, J. and Carey, W. (2010). Experimental results of a 10-element, Gatling-styled Marx generator system. 413-416. 10.1109/IPMHVC.2010.5958382.

[12] A. Lewis and L. Fegenbush. Presentation: Kraken Camera Development and Fielding, DOE/NV/03624--0924 (2020).

[13] B. Jacoby, et al., Piano Pre-Operational Report (U), COPJ-2003-0355 (2001).

[14] B. Jacoby, D. Pilkington, and T. Strand. Piano Sub-Critical Experiment Post-Operational Report (U), COPJ-2004-0209 (2004).

[15] W. M. Wood, T. J. Haines, N. S. P. King, and J. R. Smith. Measurements of Ejecta in the Barolo Experiment, Defense Review 24(3) (2010) 02166221AD.

[16] W. M. Wood. Report: Determining Relevant Particle Size Information Using Two-color Optical Transmission Measurements (2016).

Acknowledgments

The following persons contributed to this work: Duane Smalley, overall contributions to the NNSS radiography program; Jeremy Danielson, ongoing support of NNSS diagnostic efforts; Danny Sorenson, specialized shadowgraphy analysis; Bob Malone, innovative optical imaging solutions; Logan Fegenbush and the TDI camera design team, Kraken camera development; and David Phillips and Matt Lara, specialized pulsed power and x-ray source support.